SILICON WAFER DEFECT SEGMENTATION USING MODIFIED PULSE COUPLED NEURAL NETWORK

by

CHAITANYA TELIDEVARA

Presented to the Faculty of the Graduate School of

The University of Texas at Arlington in Partial Fulfillment

of the Requirements

for the Degree of

MASTER OF SCIENCE IN ELECTRICAL ENGINEERING

THE UNIVERSITY OF TEXAS AT ARLINGTON

May 2011

DEDICATION

To Amma, Nanna, Munni & Teju.

ACKNOWLEDGEMENTS

I would like to express my sincere gratitude to Dr Michael T. Manry, for supervising me on this thesis and helping me in every step of my work.

I wish to thank Dr Alan Davis and Dr Liang for taking time to serve on my thesis committee.

I would also like to thank the University Library for providing excellent templates to work with.

April 12, 2011

ABSTRACT

SILICON WAFER DEFECT SEGMENTATION USING MODIFIED PULSE COUPLED NEURAL NETWORK

Chaitanya Telidevara, M.S.

The University of Texas at Arlington, 2011

Supervising Professor: Michael T. Manry

Defect segmentation has been a focal point in silicon wafer inspection research and it remains challenging because the defects are complicated by large variations in intensity distribution. An algorithm for silicon wafer defect segmentation is developed using a modified pulse coupled neural network (PCNN). The modified PCNN is simple version of the PCNN in which segmentation depends only on the linking coefficient and initial threshold. The initial threshold and linking coefficient are determined automatically from image statistics using method described in [17] and Otsu's method respectively. The modified PCNN method was found to be simple and efficient for silicon wafer defect segmentation. The performance of the modified PCNN is better than the Otsu's method or a standalone PCNN. Results have been presented for all the four types of silicon defect.

TABLE OF CONTENTS

LIST OF FIGURES

LIST OF TABLES

CHAPTER 1

INTRODUCTION

Segmentation is a partitioning of an image into constituent parts using attributes such as pixel intensity, spectral values, and textural properties. Segmentation produces an image representation in terms of boundaries and regions of various shapes and interrelationships. Image segmentation to a large extent depends on suitable threshold values which produce binary images to produce neither under-segmentation, nor over segmentation [8]. The results of the image segmentation process are further used for object recognition and image analysis.

1.1 Application of Image segmentation

Image segmentation is used in applications such as locating objects in satellite images [16], face recognition [1], mail sorting [4], fingerprint recognition [5], target recognition [14] and brake light detection [6]. Image segmentation is used in mail sorting systems to locate various objects like stamps, addresses and barcodes. In the medical field, image segmentation is applied in tumor location [3], tissue volume measurement [44], computer guided surgery [43], diagnosis, treatment planning [45] and the study of anatomical structures [7]. In many manufacturing companies, it is essential to detect defects to ensure quality of the product [17]. Image segmentation is the major processing step in

automated detection of fabric defects [17] and foreign particle detection in injection fluid [37]. In this thesis work we are concerned with silicon defect segmentation.

1.2 Image segmentation methods and their problems

There are many different algorithms and techniques used for image segmentation. The method used depends on the application, computation complexity and the level of accuracy required. This sub-section discusses various image segmentation methods and their limitations.

1.2.1 Threshold based segmentation

Gray-level thresholding is the simplest segmentation method. Many objects or image regions are characterized by constant reflectivity or light absorption of their surfaces. Threshold can be determined to segment objects of corresponding to these region and background [19]. If object do not touch each other and if their gray-levels are clearly distinct from background gray-levels, thresholding is a suitable segmentation method [20]. Correct threshold selection is crucial for successful threshold segmentation. This selection can operate interactively or it can be the result of some threshold detection method. The simplest threshold based segmentation method is global thresholding. In global thresholding a single threshold is used for segmenting the whole image [9]. Only under a few circumstances is this method suitable for image segmentation. Images which cannot be segmented using global thresholding are often segmented using an adaptive thresholding method. Many practical segmentation applications need more information than is contained in one spectral band. To segment images, many threshold values are required. In multi-spectral satellite image segmentation, for example, a threshold is

determined independently for each channel and segmented images using these thresholds are combined into a single segmented image [20].

1.2.2 Edge based segmentation

Edge-based segmentation relies on edges found by edge detecting operators like Sobel, Prewitt and Laplacian operators [19]. These edges mark locations of discontinuities in gray-level, color, texture etc... The image obtained from edge detection cannot be directly used as a gray-level segmentation result. Supplementary processing is required to combine edges into edge chains that correspond better with borders in the image [9]. Better segmentation results are obtained if more priori information about the image is available [20]. The most common problems in edge-based segmentation are caused by image noise which results in edge detection in locations where there is no border, and no edge detection where a real border exists [19].

1.2.3 Region based segmentation

In region-based segmentation [20] image characteristics are used to map individual pixels to sets of pixels that might correspond to an object. Local techniques, global techniques and splitting and merging are various region based segmentation techniques. The area of application and the input image determine accuracy and effectiveness of the region growing algorithm used [20]. Local techniques can be effectively applied to simple images. However, for difficult images, even the most sophisticated techniques fail to produce a satisfactory segmentation. Two adjacent regions are merged if significant part of their common boundary consists of weak edges. If only one region based segmentation method with over-stringent segmentation criteria is used to avoid the merging of regions due to weak edges it creates fragmentation in regions leading to over segmentation. This

problem of merging is dealt with hybrid techniques which uses a mix of region based segmentation methods.

1.2.4 Graph partitioning methods

In graph partitioning methods [20] the goal is to model an image as a weighted, undirected graph. A pixel or a group of pixels are associated with nodes and edge weights define the similarity or dissimilarity between the neighborhood pixels [9]. The graph (image) is then partitioned according to a criterion designed to model "good" clusters. Each partition of the nodes (pixels) output from these algorithms is considered an object segment in the image. Normalized cuts, random walker, minimum cut, isoperimetric partitioning and minimum spanning tree-based segmentation are some of the popular methods in this category [19].

1.2.5 Clustering method

Clustering [15] is a process in which pixels that belong to the same color, texture etc. are grouped into a cluster. The two natural algorithms used for clustering are divisive clustering and agglomerative clustering [19]. The two major problem involved in using either of the methods is that there are lots of pixels in an image and the methods are not explicitly designed to optimize the objective function. This limitation can be overcome by writing down an objective function and then building an algorithm. The K-means algorithm [19] is an iterative technique that is used to partition an image into K clusters, where each pixel in the image is assigned to the cluster that minimizes the variance between the pixel and the cluster center and is based on pixel color, intensity, texture, and location, or a weighted combination of these factors [18]. This algorithm is guaranteed to

converge, but it may not return the optimal solution. The quality of the solution depends on the initial set of clusters and the value of K [20].

1.2.6 Knowledge based segmentation

In this approach it is assumed that structures of objects have a repetitive form of geometry [20]. Therefore, a probabilistic model is used for explaining the variation of the shape of an object in an image. Image segmentation can be done by imposing constraints using this model [9]. Three important tasks involved in this type of image segmentation are [19]:

(i) Registration of the training examples to a common pose,

(ii) Probabilistic representation of the variation of the registered samples, and

(iii) Statistical inference between the model and the image.

Knowledge-based segmentation uses active shape and appearance models, active contours and deformable templates and level-set based methods [2].

1.3 Neural network segmentation

Neural network segmentation techniques process an image using a set of neural networks [26]. After such processing the decision making mechanism marks the areas of an image accordingly to the category recognized by the neural network. Kohonen self organizing maps are used for this purpose. PCNNs are used in many image processing applications [3, 10].

The limitations of the methods discussed previously can be partially overcome using neural network based segmentation methods. The PCNN based segmentation method has several significant merits including robustness against noise, independence of geometric variations in input patterns and capability of bridging minor intensity variations in input

patterns [23]. The high level of required computation restricts it use to few application in which simple methods fail to provide reliable results.

1.4 Limitations of existing systems for silicon wafer defect segmentation

The simple image segmentation methods like thresholding, edge detection and region growing are not suitable for segmenting silicon wafer defect images since they have more complex histogram distributions and non-uniform intensity variations. Although, modified forms of these methods in conjunction with other methods yield good results for applications like fabric defect detection [17, 36], injection fluid foreign particle detection [37] and aerial target detection [39], it is difficult to find the right combination for silicon defect images. The image segmentation can be done using PCNN with suitable parameter values. These parameter values are not fixed and they depend on the type of image segmentation application [42]. So, the PCNN parameter values used for existing application are not suitable for silicon defect segmentation. Hence, a simple and reliable algorithm is required to determine the values of PCNN's parameters for segmenting silicon wafer defects.

1.5 Objective and overview of this thesis

The primary objective of the thesis is to develop a new segmentation algorithm based on a modified PCNN. The thesis is organized as follows; Chapter 2 describes four silicon defects. Chapter 3 presents a study of image segmentation using Otsu's method. Chapter 4 presents a study of image processing using PCNN. In chapter 5 a modified PCNN based on Otsu's method is developed for silicon defect segmentation. In chapter 6 results are presented comparing segmentation methods for our application.

CHAPTER 2

SILICON WAFER DEFECTS

A wafer is a thin slice of semiconductor material, such as a silicon crystal, used in the fabrication of integrated circuits and other micro devices. The wafer serves as the substrate for microelectronic devices built in and over the wafer and undergoes many micro fabrication process steps such as doping or ion implantation, etching, deposition of various materials, and photolithographic patterning [48].

Defects in silicon are one of the principle causes for rejection of silicon wafers both by the large silicon manufacturers and the IC manufacturers. "Prime wafers", which are bought from the silicon vendors may have some faults which make them unsuitable for further use [49]. Prime wafers that meet all the specifications and are suitable for device manufacture are very expensive.

There are many defects associated with silicon wafers and most are caught at the silicon manufacturer. Wafer defects range from pits in the silicon surface and tiny scratches, to things that are hidden from view, buried below the silicon surface. The defects can be captured using high resolution CCD cameras and further process them to obtain value information on various physical aspects of the defects [47]. Scanning electron microscope is used for the nondestructive inspection, evaluation and analysis of micro-structural

surfaces [46]. Silicon surface defect images used in thesis are obtained from the scanning electron microscope. The following section discusses the various defects considered in this thesis.

2.1 Types of defects

Crystalline defects in silicon can be classified into four categories according to their geometry. These categories are [46]: (1) Zero-dimensional or 'Point' defects (2) One-dimensional or 'Line' defects (3) Two-dimensional or 'Area' defects and (4) Three-dimensional or 'Volume' defects. The defects considered in this thesis are volume defects. Volume defects in a crystal are formed due to precipitation of impurity in supersaturated conditions. These precipitates are considered undesirable because they act as sites for the generation of dislocation crystal of a wafer. Precipitates induced during silicon wafer processing come from oxygen, organic contaminants, metallic impurities and dopants like boron. The four types of volume defects are considered in this thesis are copper ball defect, plastic defect, protrusion defect and pit defect.

2.1.1 Copper ball defect

Copper contamination is introduced on the silicon wafer surface during cleaning procedures or device processing. It will diffuse into the bulk at high temperature annealing and diffuses out from the bulk of wafer surface during cooling from high temperature as a result of super saturation and high diffusivity [49]. The diffused out copper contaminant can assume various morphological shapes. In this thesis work the ball shaped copper defect on silicon wafer surface is considered.

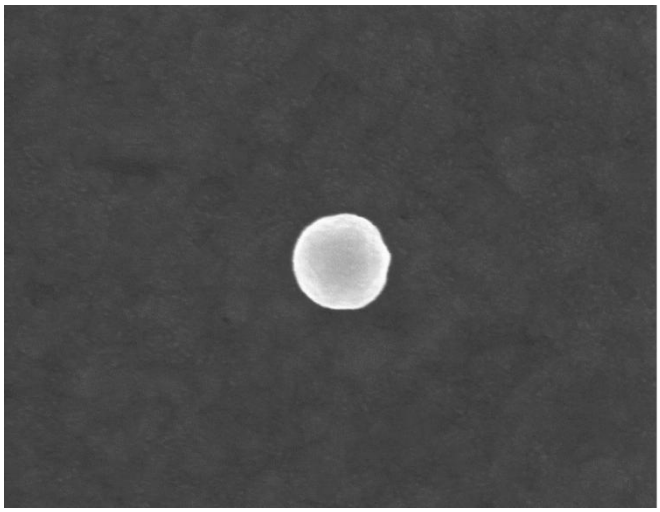

Figure 2.1 Image of silicon wafer with copper ball defect

2.1.2 Plastic defect

Plastic defects are formed due to undesirable deposition of plastic on the silicon wafer during processing. Condensation from the clean room air onto the wafer surfaces of organic vapors is primary cause of plastic contamination on the wafer. The shape of the plastic contaminant formed by condensation of vapors is irregular with thin and smooth surfaces.[46]. In the plastic defect the plastic is spread over the silicon wafer. Due to this spread, there are small variations in intensities between the defect and background regions. It is difficult to define threshold values used for segmentation using simple methods.

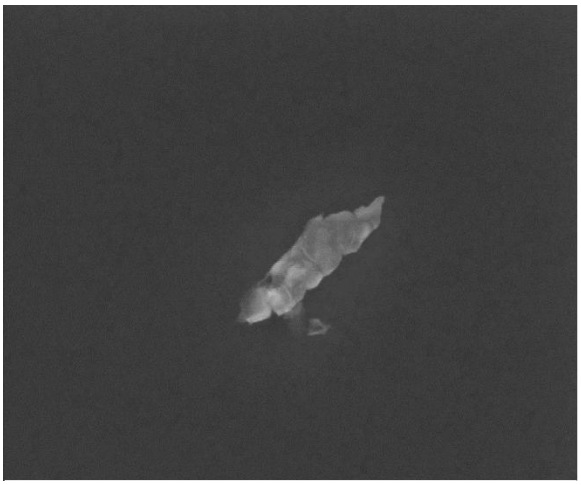

Figure 2.2 Image of silicon wafer with plastic defect

2.1.3 Protrusion defect

The root cause for protrusion defect is the expansion of a thin oxide film on the silicon surface. The defect shape is very similar to bubbles with most of them located at the round or flat site of the wafer's edge. This only happens in areas that have pre-implant oxide on silicon surface. In this thesis bubble shaped protrusions are considered [47].

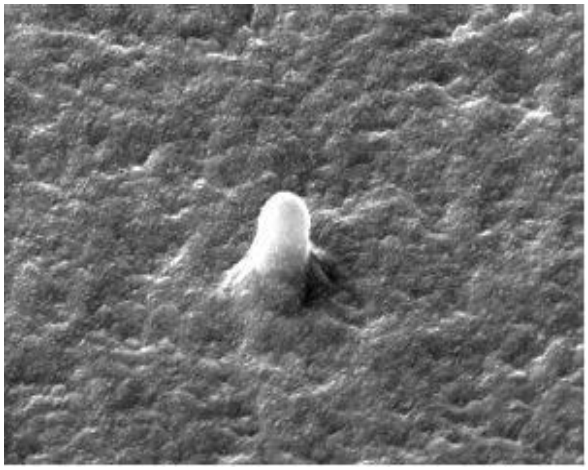

Figure 2.3 Image of silicon wafer with protrusion defect

2.1.4 Pit defect

Pit defects on silicon wafers are formed during hydrogen annealing. Faceted pyramidal pits are due to anisotropic etching and the rounded pits are isotropic etching due to

thermodynamic property change of silicon surface as a function of temperature [48]. In this thesis, rounded pit defects are considered.

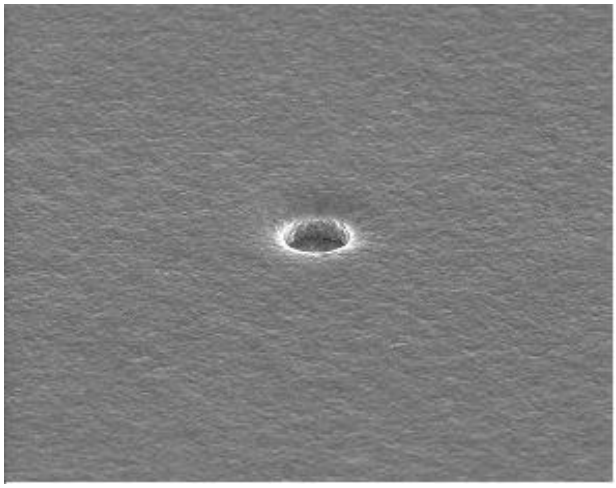

Figure 2.4 Image of silicon wafer with pit defect

2.2 Problems involved in segmentation of silicon defects

2.2.1 Non-uniform gray-level variations

Non-uniform input device parameters and number of other factors cause gray-level variations in objects and background. The images of this kind cannot be segmented using global thresholding methods. Adaptive thresholding is the other thresholding approach used for these images. In adaptive thresholding methods, variable thresholds obtained from local characteristics of an image are used for segmentation.

2.2.2 Threshold selection for defect segmentation

Threshold value selection is a complex task in silicon defect segmentation. A large variation in the intensity distribution and the presence of varying range of defect regions in these images are factors which make threshold selection a difficult task. These factors are different for different types of defects making it difficult to rely on single method for

segmentation. The segmentation of all these defects can be tried using methods which are capable of selecting good threshold values and capturing the defect region efficiently.

2.2.3 Variations in defect region

In addition to the spread of the defect regions in a silicon wafer image, there is a large variation in intensity values in these regions. To segment the defects in the images many threshold values are required and the pixels corresponding to these defects should be connected based on some criteria. Connection of pixels of this defected region makes it easy to estimate the spread of the particular defect.

2.3 Goal of this thesis

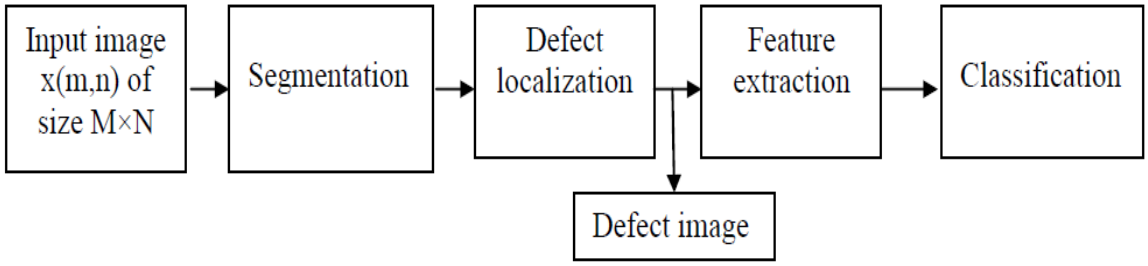

Figure 2.5 Schematic diagram of the defect recognition system

Defection recognition is one of the requirements for the quality assurance in manufacturing industries [17]. Figure 2.5 depicts the schematic representation of the silicon defect recognition system. This system consists of five components: (1) Input image x(m,n) of size M by N (2) Segmentation (3) Defect localization (4) Feature extraction and (5) Classification. The segmentation block is important, as further processing is dependent on the results of this block. Efficient and automated segmentation is a major requirement of this system .The goal in the remainder of this thesis is to develop a reliable and automated segmentation algorithm using a modified

PCNN. The results from segmentation are processed to localize the defects. There can be defects of different sizes and morphology in the same image. Localization of the defect is useful because features for the different defects in the same image can be extracted and classified. The procedure involved in the localization of the defect is explained in detail in the following sub section.

2.4 Defect localization

The localization of the defects in the binary images obtained after segmentation involves three steps: (1) Computation of connected components (2) Finding the defects with area more than a predefined value and (3) Obtaining a box that encloses the defect.

2.4.1 Computation of connected components

A segmented, M by N binary image y(m,n) is input to the connected component algorithm [20]. The output image obtained is a labeled image L(m,n) of size M by N in which pixel values are labeled. The purpose of calculating connected components is to group the defects present in the segmented image and to label them so that they can be used for localization. In this thesis, a recursive labeling algorithm [20] is used for computation of connected components. Firstly, all pixels with value 1 are changed to -1. This step is needed to distinguish unprocessed pixels (i.e with value -1) from those of processed pixels with component label 1. The next step is to assign the smallest pixel with value -1, a new label and searching for the neighboring pixels whose value is -1. This step is repeated for the neighboring pixels until all pixels are labeled. The resultant output image with labeled pixels is saved as the labeled image L(m,n).

2.4.2 Finding defects greater than predefined area

The area of the defects labeled in the previous step is calculated as the number of pixels occupied by the defect. For each labeled defect determine the starting pixel and ending pixel. Determine area of the defect by counting number of pixels between starting pixel and ending pixel with same labels. Defects with areas less than the predefined value are eliminated by making the value of pixels of the defect equal to 0 in the segmented image.

2.4.3 Drawing a rectangle around the defect

The defects filtered in the previous step based on their area are the defects of interest. For further processing of these defects they should be localized. This localization of the defect is done in this thesis by obtaining a box that encloses the defect. The starting pixel and ending pixel of each defect are determined. The vertices of the box are determined based on dimensions obtained from starting and ending pixel.

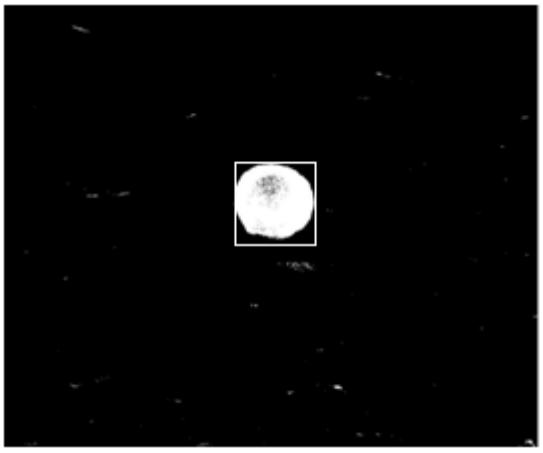

Figure 2.6 Image showing localized defects

A copper ball defect enclosed in a box is shown in figure 2.6. This image is obtained after processing a segmented image. The defect localized image highlights the defects and can be further processed for feature extraction and recognition.

CHAPTER 3

OTSU'S METHOD

Selection of a correct threshold of gray level for extracting objects from background is important for defect segmentation. Various techniques were proposed for selection of this threshold. In an ideal case, the histogram has a deep and sharp valley between two peaks representing objects and background, respectively, so that the threshold can be chosen at the bottom of this valley [36]. It is difficult to determine the bottom of the valley for flat and broad valleys with the peaks of extremely unequal in height [37]. This limitation is overcome by using method proposed by the Japanese scholar Otsu [19] which is based on the class variance. In this method the best threshold is selected using the largest interclass variance between the objects and the background.

3.1 Image segmentation using Otsu's method

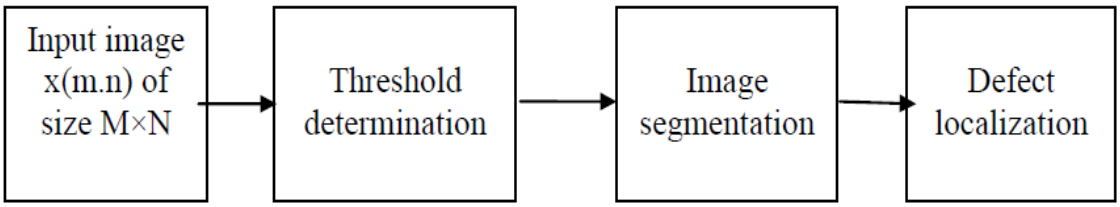

Figure 3.1 Schematic diagram of system based on Otsu's method

Otsu's method is a simple threshold based image segmentation method in which the threshold value is determined. The threshold value is used to segment the whole image into two regions, one region corresponding to the objects and other corresponding to background.

Image segmentation using Otsu's method consists of three steps: (1) Threshold determination (2) Image segmentation and (3) Defect localization. These steps are discussed in detail in the following subsections.

3.1.1 Threshold determination using Otsu's Method

The threshold is determined based on discriminate analysis in which the threshold operation is regarded as the partitioning of the pixels of an image into two classes. Pixels belonging to background class C_b have intensity values in the range 0 to k and pixels belonging to object class C_o have intensity values in the range k+1 to 255.

Otsu's algorithm for determination of thresholds is as follows:

(1) Calculate the probability of occurrence of pixels at intensity level i as

$$P_i = \frac{n_i}{n} \tag{3.1}$$

where n_i is the number of pixels with grey level intensity i and n is the total number of pixels

(2) Initialize threshold k to 1, array η of size 255 to 0.

(3) Calculate the probabilities of class occurrence as

$$w_b(k) = \sum_{i=0}^{k} P_i \tag{3.2}$$

$$w_o\,(k) = 1 - w_b(k) \tag{3.3}$$

(4) Calculate total mean of an original image and class means as

$$\mu_T = \sum_{i=0}^{255} i \cdot P_i \tag{3.4}$$

$$\mu_b\,(k) = \frac{1}{w_b(k)} \sum_{i=0}^{k} i \cdot P_i \tag{3.5}$$

$$\mu_o\,(k) = \frac{1}{w_o(k)} \sum_{i=k+1}^{255} i \cdot P_i \tag{3.6}$$

(5) Calculate class variances as

$$\sigma_b(k)^2 = \frac{1}{w_b(k)} \sum_{i=1}^{k} (i - \mu_b\,(k))^2 \cdot P_i \tag{3.7}$$

(6) Calculate within class, between class and total variances respectively as

$$\sigma_W(k)^2 = w_o(k) \cdot \sigma_o(k)^2 + w_b(k) \cdot \sigma_b(k)^2 \tag{3.9}$$

$$\sigma_B(k)^2 = w_o(k) \cdot (\mu_o\,(k) - \mu_T\,)^2 + w_b(k) \cdot (\mu_b\,(k) - \mu_T\,)^2 \tag{3.10}$$

$$\sigma_T^2 = \sum_{i=1}^{255} (i - \mu_T\,)^2 \cdot P_i \tag{3.11}$$

(7) Calculate the discriminant criterion measure parameter for threshold k as

$$\eta(k) = \frac{\sigma_B(k)^2}{\sigma_T^2} \tag{3.12}$$

(8) k=k+1.If k≤255 go to step 3 else go to step 9.

(9) Select the maximum value in the array η and save the corresponding threshold as Otsu's method threshold t.

$$t = \max_{1 \le k \le 255} \eta(k) \qquad (3.13)$$

3.1.2 Segmentation algorithm

The algorithm for image segmentation based on Otsu's method threshold is as follows

Step 1: Initialize output image array y of size M×N to 0, m and n to1.

Step 2: Compare the intensity of pixel (m, n) in a given image with the threshold t calculated in previous section. Assign the value to y(m,n) as

$$y(m,n) = 0 \; if \; x(m,n) < t$$

$$y(m,n) = 1 \; if \; x(m,n) \geq t$$

Step 3: n=n+1. If n≤N go to step 2,else go to step 4.

Step 4: n=1,m=m+1. If m≤M go to step 2,else go to step 5.

Step 5: Save image **y** as the segmented image.

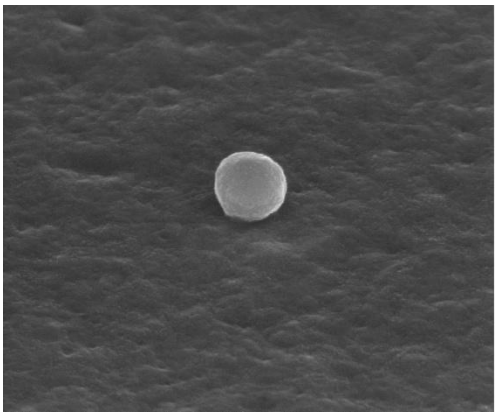

Figure 3.2 Original image

An input image with a copper ball defect is shown in figure 3.2. It can be observed that intensities of defect pixels are higher than those of background pixels, which results in a bimodal histogram distribution allowing effective segmentation using Otsu's method.

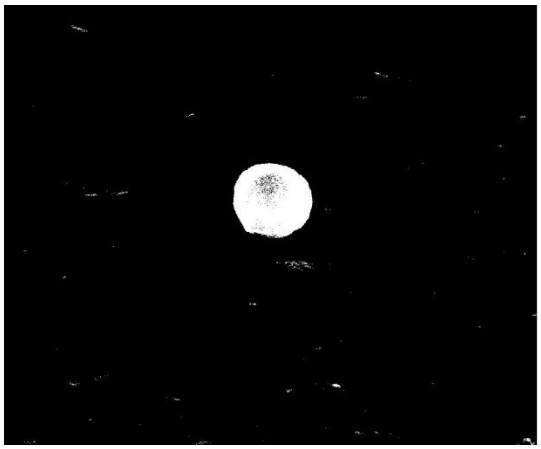

Figure 3.3 Segmented image obtained using Otsu's method

The segmented image of figure 3.3 clearly shows the defect present in the silicon image. These defects are localized to highlight the defect region.

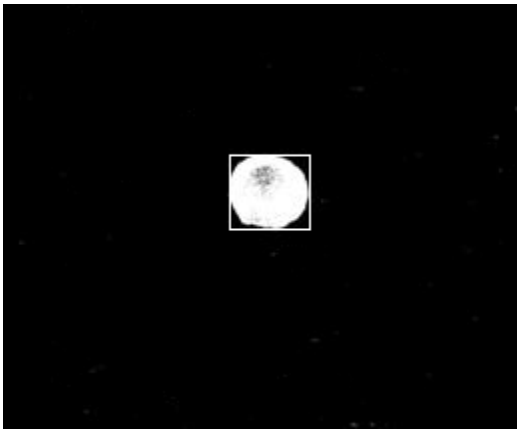

Figure 3.4 Image showing localized defects

The localized defect of figure 3.4 is obtained using the method described in section 2.4 with the segmented image as input. In figure 3.4 the defect is highlighted and can be further processed to extract features useful for recognition.

3.2 Problems with Otsu's method

Otsu's method is suitable for simple images in which the histogram has a bimodal distribution [19]. Unfortunately, complex images with varying intensity distributions do not have a clear bimodal histogram. In addition to this, image segmentation using Otsu's

method yields better results for high quality images with stable background. Noise present in the images significantly influences the results obtained using this segmentation method. So, Otsu's method should be used after denoising the image and should be modified based on the application. An algorithm which can adaptively determine the threshold value based on the image characteristics is required to segment these images.

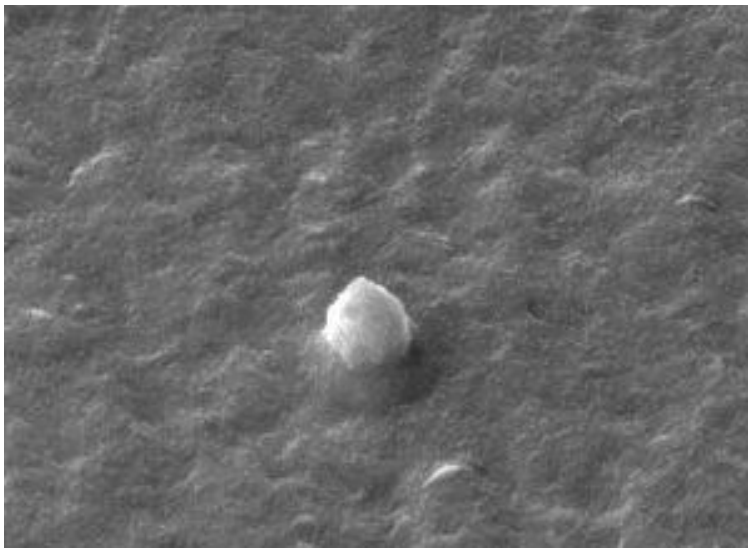

Figure 3.5 Original image

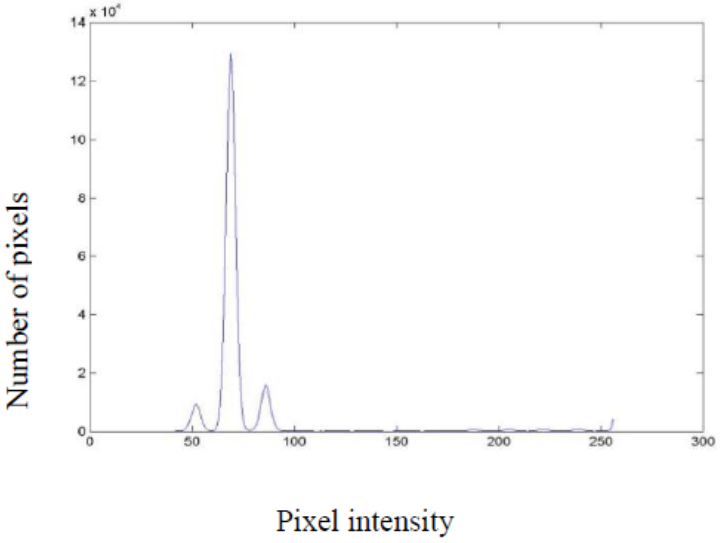

Figure 3.6 Histogram

The image shown in figure 3.5 has a protrusion defect. It can be observed that there is a large variation in intensities between the defect and background pixels. The histogram of this image in figure 3.6 clearly depicts sharp peaks and deep valleys. The higher number of pixels in lower intensity region corresponds to background and the lower number of pixels in higher intensity regions corresponds to the defect. Otsu's method works effectively for this image because of the presence of sharp peaks and valleys.

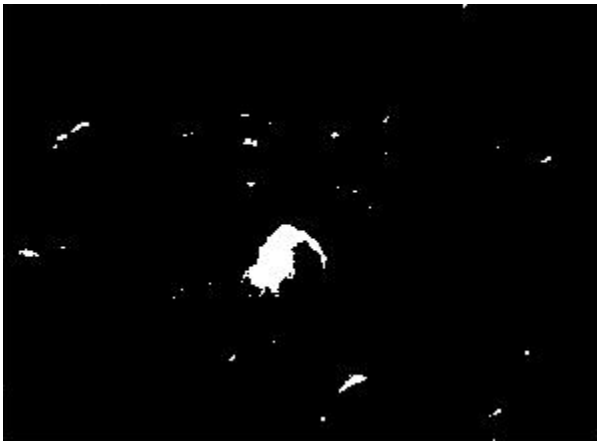

Figure 3.7 Segmented image obtained using Otsu's method

The defects present in input image are highlighted in figure 3.7 showing effective segmentation of the defect using Otsu's method.

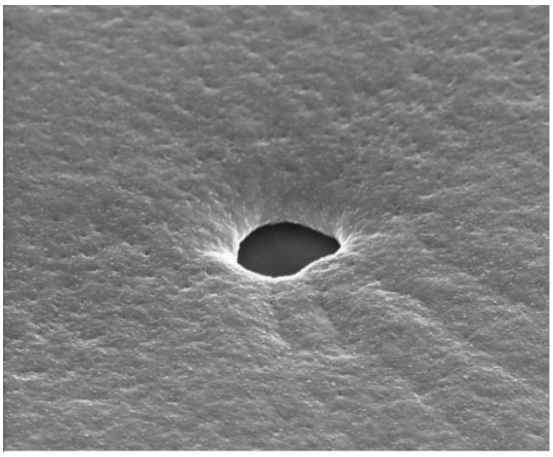

Figure 3.8 Original image

An input image containing a pit defect is shown in figure 3.8. Here the variation of ntensities is not as large as compared to copper ball defect image shown in figure 3.5. This makes it difficult to segment using Otsu's method

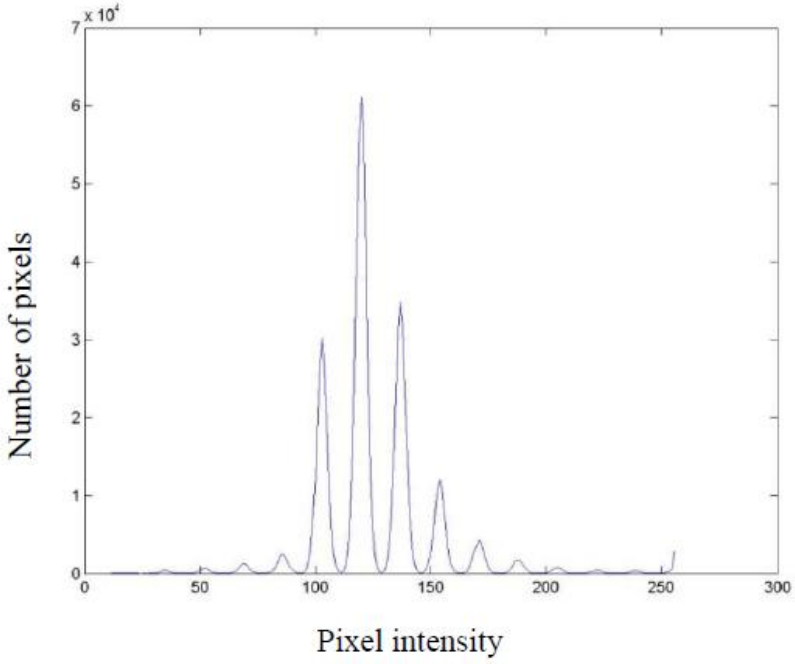

Figure 3.9 Histogram of original image

In contrast to this the histogram of silicon image defect shown in figure 3.6, histogram shown in figure 3.9 is a multimodal distribution with many peaks and valleys which make it difficult to segment. Hence, Otsu's method fails to segment the image shown in figure 3.8.

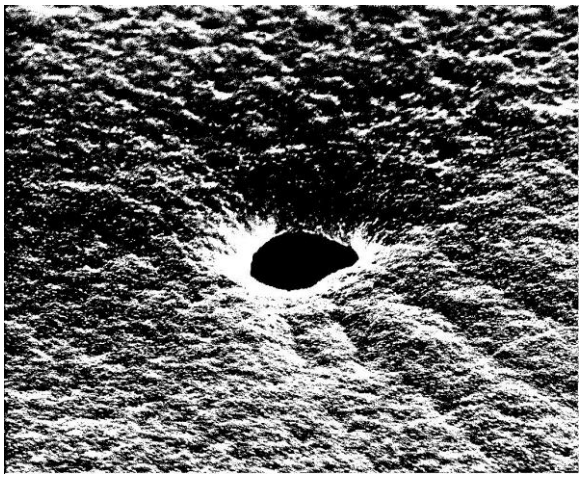

Figure 3.10 Failed image segmentation

A segmented pit defect image is shown in figure 3.10. It can be observed that Otsu's method has failed to correctly segment the defect. This failure is due to the multimodal distribution of intensities in input image figure 3.8.

The defects in a silicon wafer image can range from small defects to large defects. The corresponding histograms can be unimodal or multimodal. Otsu's method cannot segment all these defects and an improved Otsu's approach like the valley-emphasis method [36] could be tried. However, the improved Otsu's approach gives better results only for images with unimodal or bimodal intensity distribution. Defects like the pit defect shown in figure 3.8 with multimodal intensity distribution can be segmented using PCNN which is discussed in following chapter.

CHAPTER 4

PULSE COUPLED NEURAL NETWORK

The mammalian visual system is more complicated and efficient than a computer based image processing and recognition systems. In mammalian systems, decisions on the content of an image are made after performing many operations in the visual cortex. This processing capability cannot be achieved in computer based systems using simple processing algorithms. However, this can be achieved by computer algorithms which are capable of emulating the processes of the mammalian visual cortex [23].

Eckhron's neuron model developed in 1990's is based on the experimental observation of synchronous pulse bursts in the cat and monkey visual systems [22]. Eckhron's neural networks, through stimulus forced and stimulus induced synchronization, are able to bridge temporal gaps and minor magnitude variations in input data and cause the neurons with similar inputs to pulse together. This neuron model will group image pixels based on spatial proximity and brightness similarity.

The PCNN is obtained by making minor modifications to the Eckhron's model to make it suitable for image processing applications. The results obtained from PCNN image processing are invariant to image that were shifted, rotated, scaled and skewed. This

working mechanism of PCNN makes it reliable system for image processing and recognition applications.

PCNN [23] is a two-dimensional, high performance neural network used for image processing applications such as image segmentation [10], image denoising, feature extraction [25] and pattern recognition, image enhancement [27, 28, 29] and image fusion [33]. Image denoising, image enhancement, image fusion refer to applications in image preprocessing. Image denoising and image segmentation are two major steps involved in silicon defect segmentation. These two processes are discussed explicitly in the following sub-sections.

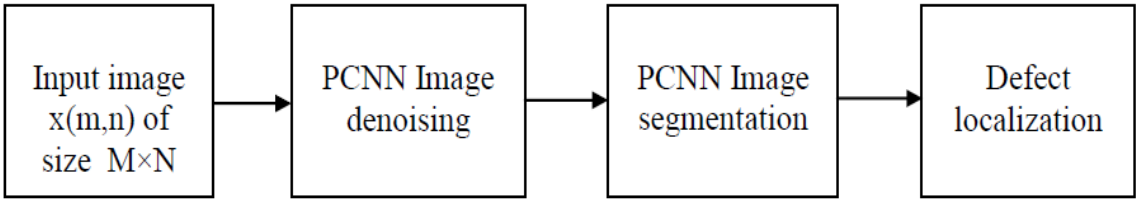

Figure 4.1 Schematic diagram of silicon defect image processing using PCNN

4.1 Image denoising using PCNN

Image denoising is the process of removing or reducing random noise present in images. The PCNN used for image denoising consists of three compartments: (1) Input compartment (2) Modulation compartment and (3) Output compartment [20].

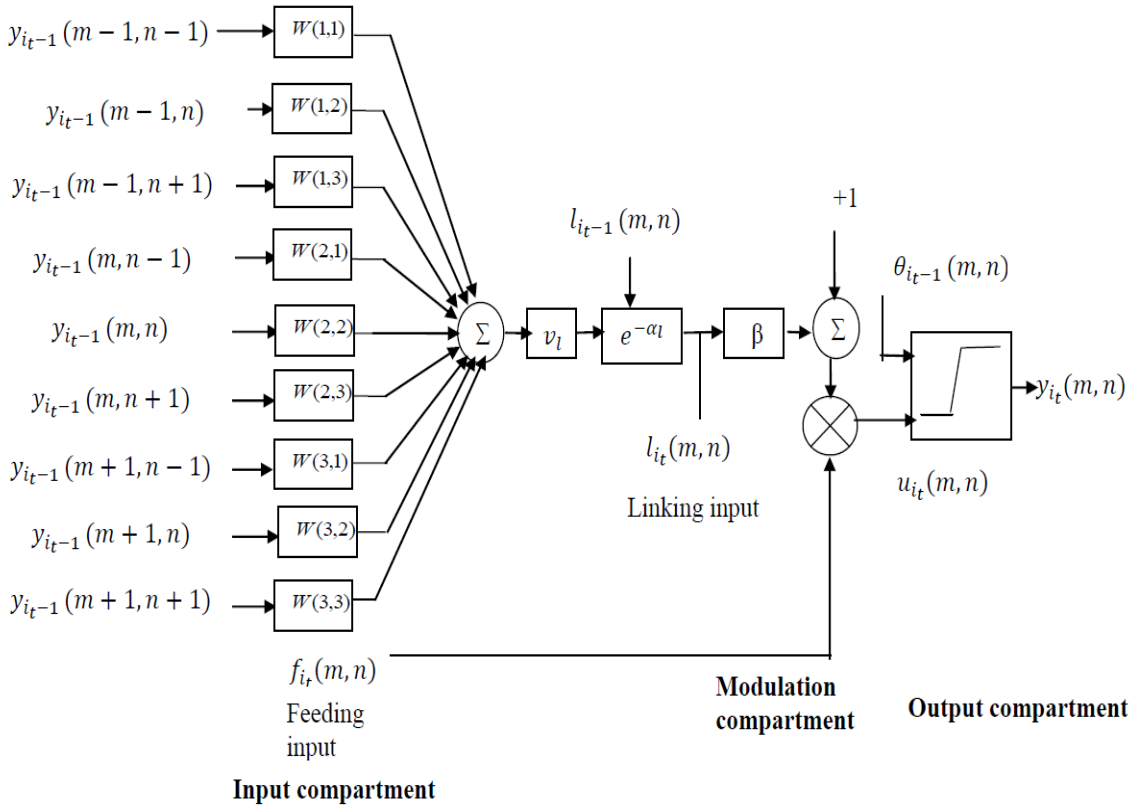

Figure 4.2 Schematic diagram of PCNN used for image denoising

Input compartment: The input compartment for pixel x(m,n) consists of two inputs: (1) the feeding input $\mathrm{f_{i_t}(m,n)}$ and (2) the linking input $\mathrm{l_{i_t}(m,n)}$. The feeding input is a combination of the intensity of image pixel x(m,n), the feeding input from a previous iteration $\mathrm{f_{i_t-1}(m,n)}$ (which is equals for the first iteration) and weighted sum of 3×3 neighborhood outputs from previous iteration $\mathrm{y_{i_t-1}(m,n)}$ determined

$$f_{i_t}(m,n) = \begin{cases} \frac{1}{8}\sum_{i=-1}^{1}\sum_{j=-1}^{1} x(m+i,n+j) & if\ \ y_{i_t-1}(m,n)=0 \\ x(m,n) + f_{i_t-1}(m,n) + v_f \cdot \sum_{i=-1}^{1}\sum_{j=-1}^{1} W(i+2,j+2)\cdot y_{i_t-1}(m+i,n+j) & otherwise \end{cases} \quad (4.1)$$

where **W** is the weight matrix for 3×3 neighboring pixels, α_f is the decay constant for feeding input $f_{i_t}(m, n)$ and v_f is the magnitude scaling term for feeding input.

The weighted sum of outputs from a previous iteration of 3×3 neighboring image pixel intensities is the linking input. The linking input is determined by

$$l_{i_t}(m,n) = e^{-\alpha_l} \cdot l_{i_t-1}(m,n) + v_l \cdot \sum_{i=-1}^{1} \sum_{j=-1}^{1} W(i+2, j+2) \cdot y_{i_t-1}(m+i, n+j) \tag{4.2}$$

where α_l is the decay constant for linking input $l_{i_t}(m, n)$ and v_f is the magnitude scaling term for linking input.

Modulation compartment: In the modulation compartment the feeding and linking inputs are combined in a second order form to calculate the internal activation $u_{i_t}(m, n)$ of the neuron associated with the pixel under consideration. This combination is controlled by the linking strength β. The internal activation is calculated as

$$u_{i_t}(m,n) = f_{i_t}(m,n) \cdot (1 + \beta \cdot l_{i_t}(m,n)) \tag{4.3}$$

The intensity of noisy pixel is significantly different from the intensities of the pixels surrounding the noisy pixel. So for image denoising, a small value for linking factor β is considered to avoid the strong linking between noisy pixel and the pixels surrounding it. Hence, the weakly linked pixel has low internal activation, which is less than the dynamic threshold $\theta_{i_t-1}(m,n)$ making the output of the pixel equal to 0.

Output compartment: Image thresholding operation and dynamic threshold $\theta_{i_t}(m, n)$ calculation is done in the output compartment. The output and dynamic threshold for the (m, n) pixel are determined as

$$y_{i_t}(m,n) = \begin{cases} 1 \text{ if } u_{i_t}(m,n) \geq \theta_{i_t-1}(m,n) \\ 0 \; otherwise \end{cases} \tag{4.4}$$

$$\theta_{i_t}(m,n) = \theta_{i_t-1}(m,n) \cdot e^{-\alpha_\theta} + v_\theta \cdot y_{i_t}(m,n) \quad (4.5)$$

where α_θ is the decay constant for dynamic threshold $\theta_{i_t}(m,n)$ and v_θ is the scaling term for dynamic threshold.

The algorithm used for image denoising using PCNN is described below.

Step 1: Initialization:

(a) Initialize values of arrays f, l, u, θ and y of size M×N to 0 (i.e. for n=0).

(b) Weight matrix[8] $\mathbf{W}=\begin{bmatrix} 0.5 & 1 & 0.5 \\ 1 & 0 & 1 \\ 0.5 & 1 & 0.5 \end{bmatrix}$

(c) Initialize network parameters [8]: $\beta=0.4$, $\alpha_f=0.3$, $\alpha_l=0.3$,$\alpha_\theta=0.3$, $v_f=0.05$, $v_l=1$, $v_\theta=20$ maximum number of iterations $N_{it}=10$, iteration number $i_t=1$, row and column variable m and n to 1.

Step 2: Calculate the feeding input and linking input using equations (4.1) and (4.2)

Step 3: Calculate the internal activation value using equation (4.3)

Step 4: Calculate the output and dynamic threshold using equation (4.4) and (4.5).

Step 5: n=n+1. If $n \leq N$ go to step 2,else go to step 6.

Step 6: n=1,m=m+1. If $m \leq M$ go to step 2,else go to step 7.

Step 7: $i_t = i_t + 1$, m=1, n=1. If $i_t \leq N_{it}$ go to step 2, else go to step 8.

Step 8: Save array **f** as the denoised image.

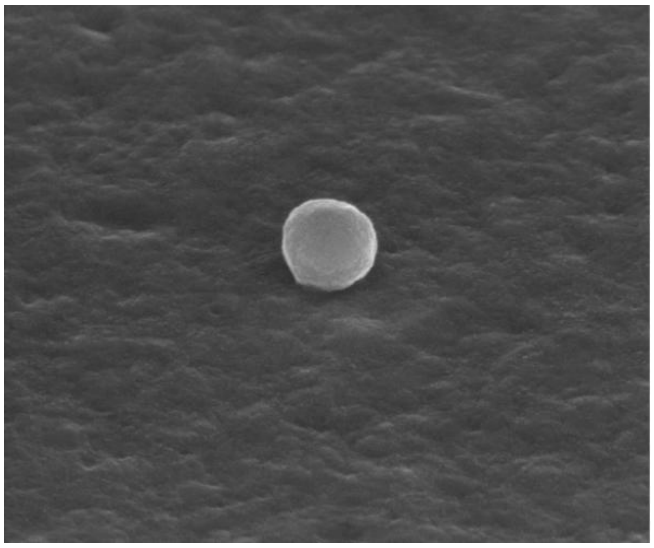

Figure 4.3 Original image

The copper ball defect image of figure 4.3 contains impulsive noise which should be removed to make it suitable for segmentation [19].

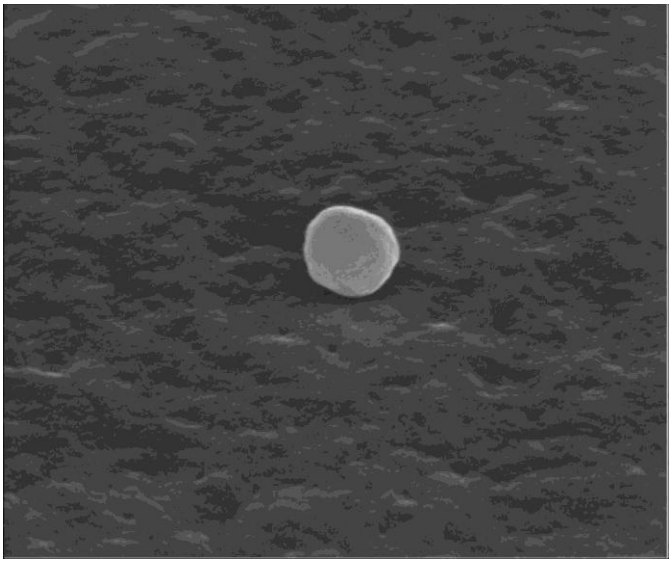

Figure 4.4 Denoised image obtained using PCNN

After denoising via the PCNN, the image of figure 4.4 results. The denoised image is suitable for segmentation [20].

4.2 Image segmentation using PCNN

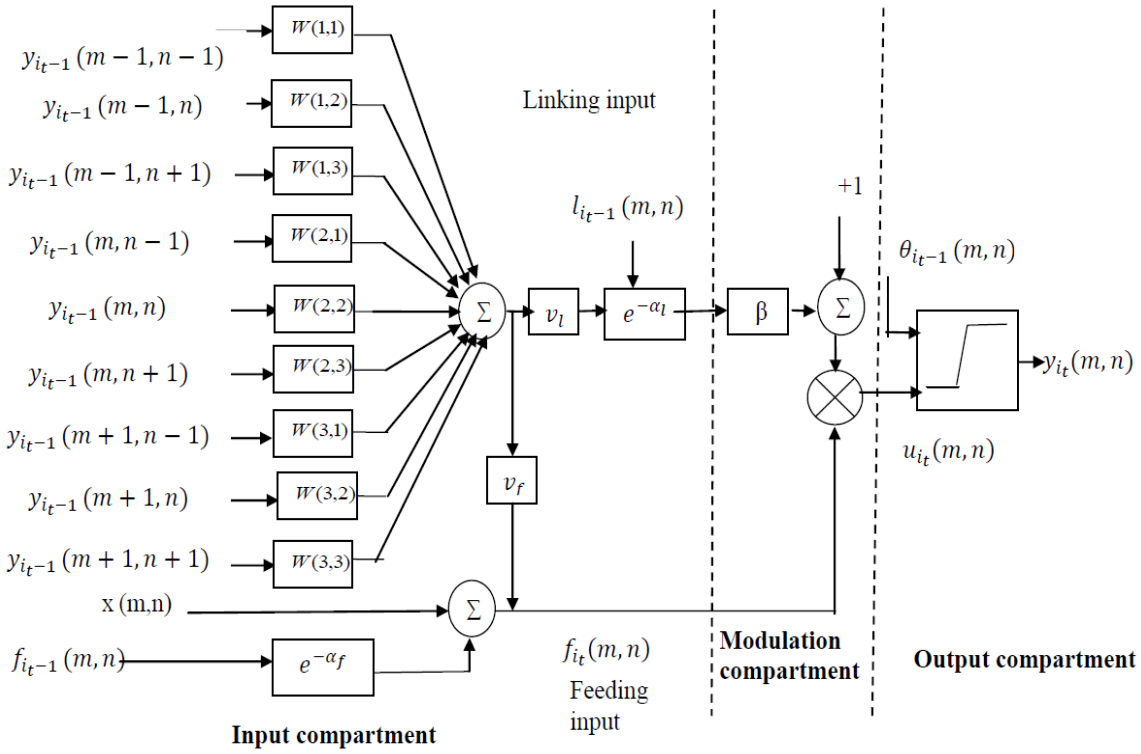

Figure 4.5 Schematic diagram of PCNN used for image segmentation

The PCNN used for the image segmentation is similar to PCNN used for image denoising but with a different feeding input equation [19]. The feeding input for the image segmentation process is determined as

$$f_{i_t}(m,n) = x(m,n) + e^{-\alpha_f} \cdot f_{i_t-1}(m,n) + \; v_f \cdot \sum_{i=-1}^{1} \sum_{j=-1}^{1} W(i+2, j+1) \cdot y_{i_t-1}(m+i, n+j) \quad (4.6)$$

Here, the input image x(m,n) for the image segmentation is the denoised image obtained in the previous section. The algorithm used for image segmentation using PCNN is described below.

Step 1: Initialization:

Initialize values of arrays f, l, u, θ and s of size M×N to 0 (i.e. for n=0).

Initialize weight matrix[8] $\mathbf{W}=\begin{bmatrix} 0.5 & 1 & 0.5 \\ 1 & 0 & 1 \\ 0.5 & 1 & 0.5 \end{bmatrix}$

Initialize network parameters [8]: $\beta=0.4$, $\alpha_f=0.3$, $\alpha_l=0.3$,$\alpha_\theta=0.3$, $v_f=0.05$, $v_l=1$, $v_\theta=20$ maximum number of iterations $N_{it}=10$, iteration number $i_t=1$, row and column variable m and n to 1.

Initialize the iteration number $i_t=1$, row and column variable m and n to 1.

Step 2: Calculate the feeding input and linking input using equations (4.6) and (4.2).

Step 3: Calculate the internal activation value using equation (4.3).

Step 4: Calculate the output and dynamic threshold using equation (4.4) and (4.5).

Step 5: m=m+1,n=n+1. If m≤M and n≤N go to step 2,else go to step 6.

Step 6: $i_t = i_t +1$, m=1,n=1. If $i_t \leq N_{it}$ go to step 2, else go to step 7.

Step 7: Save array **S** as the segmented image.

The localization of the defect is similar to one discussed in silicon defect segmentation using Otsu's method.

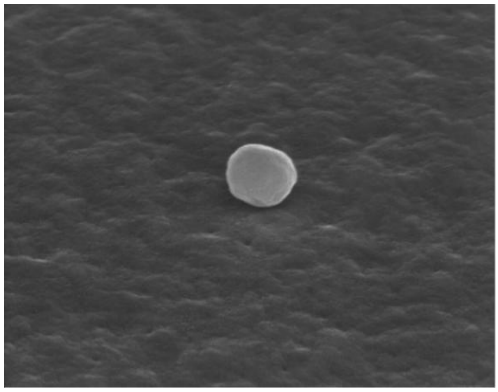

Figure 4.6 Original image

Input image with copper ball defect used for segmentation is shown figure 4.6.This image is obtained after denosing image shown in figure 4.4.

Figure 4.7 Segmented image obtained using PCNN

PCNN segmented image with copper ball defect is shown in figure 4.7. It can be seen that the defect is more clear than in the segmented image from Otsu's method in figure 3.3.

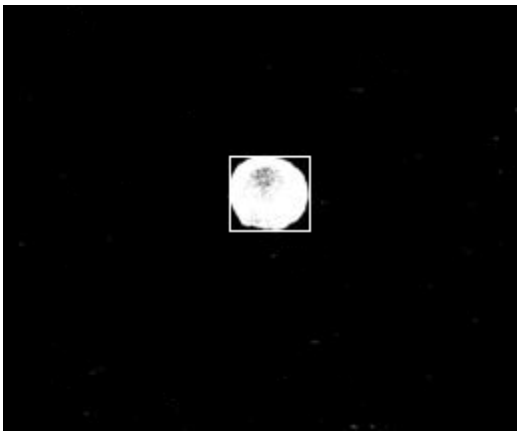

Figure 4.8 Defect localized image

The localized defect of figure 4.7 is shown in figure 4.8. The quality of the localization for PCNN method is better than that from Otsu's method.

4.3 Problems involved in using PCNN

PCNN has two major properties: dynamic threshold variation and linking with neighboring neurons. These two properties are useful in segmenting complex images with

varying intensity distributions [23]. The major constraint in using PCNN for image segmentation is selection of correct values for the network parameters $\alpha_{F,}$ α_{θ}, $\beta_{,}$ which vary for different defect images [42]. These parameters are not automatically selected in the PCNN and a suitable algorithm for determining them is required for reliable segmentation. There is no stop mechanism in the pulse coupled neural network which makes it difficult to restrict the under or over segmentation of the image [23].

CHAPTER 5

MODIFIED PULSE COUPLED NEURAL NETWORK

The accuracy of the image segmentation using PCNN of chapter 4 depends on the network parameters namely the feeding decay constant α_f, the dynamic threshold decay constant α_θ, threshold constant v_θ , linking coefficient β and stop mechanism used for determining the optimal segmented image. However, no method has been suggested for the automatic determination of these parameters from image statistics. In this chapter the PCNN of chapter 4 is modified to (1) make image segmentation depend only on the linking coefficient β and initial threshold $\theta_0(m,n)$ and to (2) include automated determination of these parameters from image statistics. The initial threshold and linking coefficient are determined using Otsu's method and a method described in [17] respectively.

5.1 Overview of block segmentation

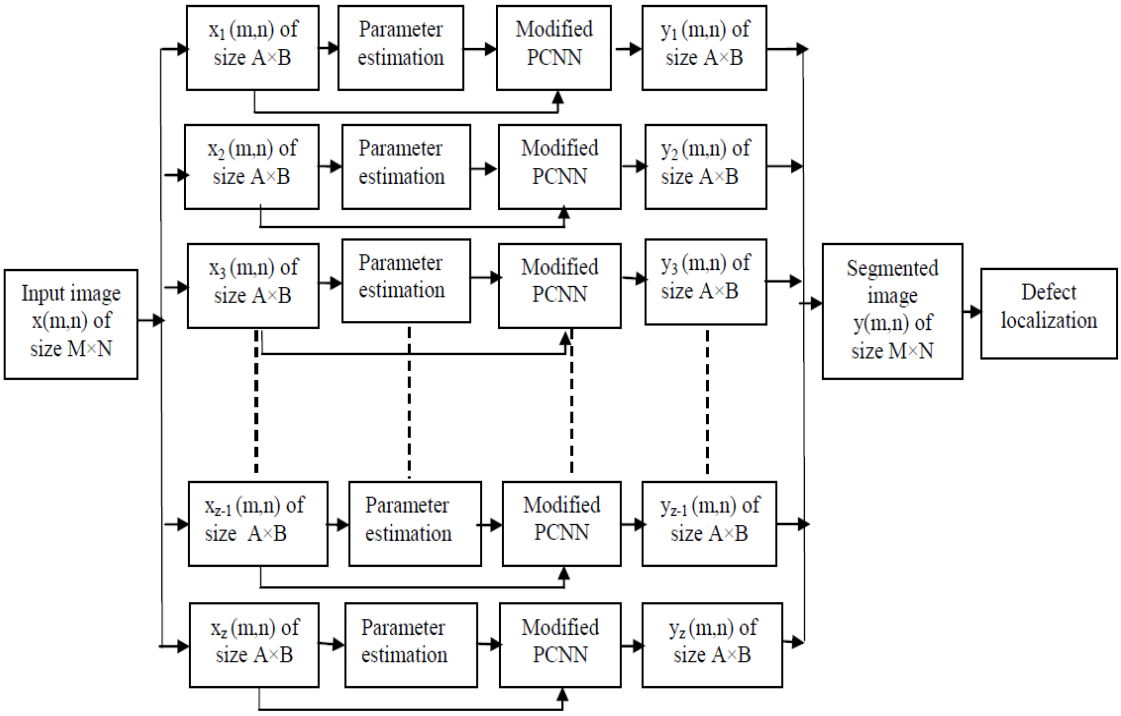

Figure 5.1 Block segmentation of an image

The problems involved in segmenting the silicon defect images described in sec 2.2 make it impractical to apply global parameters for the image. In such cases it is necessary to adapt the parameter values to match local image properties. In this thesis, block segmentation method is used in which parameter value adapt to the block properties. The steps involved in block segmentation of an image using modified PCNN: (1) Dividing image into blocks (2) Parameter estimation (3) Modified PCNN segmentation and (4) Merging of segmented blocks. In first step of block segmentation method an input image x(m,n) of size MxN is divided into blocks of sub images x_z (a,b) of same size AxB. In second step, network parameters linking coefficient β(m.n) and initial threshold θ_0(m,n) are determined. In third step, the blocks from step one are segmented separately using modified segmentation method with parameters determined in step two to obtain

segmented block images $y_z(a,b)$ of size AxB. In final step, the segmented image of each block is merged to obtain the segmented image y(m,n) of size MxN of the input image x(m,n) of size MxN. The parameter estimation and modified PCNN segmentation methods are explained in following sections.

5.2 Parameter Estimation

The segmentation results obtained using PCNN depends on the values of the networks parameters [10]. It is important to develop a method for the automatic determination of appropriate values for all PCNN parameters based on the image statistics. In this thesis, two parameters of modified PCNN: (1) linking coefficient β(m.n) and (2) initial threshold θ_0(m,n) are automatically determined from the image statistics.

5.2.1 Calculation of linking coefficient

It was observed that the PCNN method is suitable for silicon defect image segmentation as the defect occupies a small part of the image when compared to the background and has large intensity variations in the defect region. Large intensity variations in defect region problem can be dealt with linking property of PCNN [9]. In general linking coefficient β suitable for one part of the image may not be suitable for the other parts also, for effective segmentation different linking coefficient should be used for different pixels [17]. Using different linking coefficient β(m,n) gives effective segmentation results as linking depends on neighborhood grayscales distribution and similarity in grayscales values. In this thesis, different linking coefficient β(m,n) for different pixels is determined using method described in [17]. The equation for determining linking coefficient β(m,n) is given as

$$\beta(m,n) = \frac{\sqrt{\sigma(m,n)}}{1+\mu(m,n)} \quad (5.1)$$

where $\sigma(m,n)$ and $\mu(m,n)$ are variance and mean of grayscale values of 3x3 neighborhood pixels of pixel (m,n) respectively.

5.2.2 Calculation of initial threshold value

Block effect was observed in segmented image obtained using PCNN block segmentation in which initial threshold value is determined by Otsu's method. Due to block effect, some of the background regions are also segmented as object regions which resulted in non-uniform segmentation of the image. In silicon defect images there is large variation in Otsu's threshold values of sub images surrounding the defect which leads to block effect in segmented images. The block effect might result in improper localization of the defect as background regions are also identified as defect regions. The block effect can be overcome by varying the threshold value for each sub image uniformly depending on both sub image statistics and image statistics. In this thesis, both block effect and automated determination of initial threshold $\theta_0(m,n)$ problems are dealt with using combination of Otsu's method and the localized deviation of contrast parameter described in [18] .

The algorithm for determining initial threshold values of each sub image using combination of localized deviation of contrast parameter [18] and Otsu's method is as follows:

Step 1: Compute the maximum, minimum and median values of grayscales for each row and column in z^{th} sub image and denote them as r_{max} , r_{min} , r_{med} , c_{max} , c_{min} and c_{med} respectively.

Step 2: Calculate the four contrast parameters as

$$r_1 = \frac{r_{min}}{r_{max}} \tag{5.2}$$

$$r_2 = \frac{r_{med}}{r_{max}} \tag{5.3}$$

$$c_1 = \frac{c_{min}}{c_{max}} \tag{5.4}$$

$$c_2 = \frac{c_{med}}{c_{max}} \tag{5.5}$$

Step 3: Select a defect free region (which assumed to starting 10x10 block for silicon defect images) and compute the four contrast parameters using equations (5.2), (5.3), (5.4), (5.5) and denoted them r_{t1}, r_{t2} , c_{t1} and c_{t2} respectively.

Step 4: Calculate the localized deviations of contrast parameter $g_z(a,b)$ for the z^{th} sub image as[17]

$$g_z(a,b) = \frac{|r_1 - r_{t1}|}{r_{t1}} + \frac{|r_2 - r_{t2}|}{r_{t2}} + \frac{|c_1 - c_{t1}|}{c_{t1}} + \frac{|c_2 - c_{t2}|}{c_{t2}} \tag{5.6}$$

Step 5: Initial threshold value for sub image $x_z(a,b)$ is determined by [17]

$$\theta_0(a,b) = g_{max}(a,b) * \frac{t_{max}(a,b)}{g_z(a,b)} \tag{5.7}$$

where $t_{max}(a,b)$ denotes the maximum value of the threshold values of all sub images is calculated using Otsu's method and $g_{max}(a,b)$ denotes the maximum value of the localized deviations of contrast parameter.

$$t_{max}(a,b) = \max_{1 \le z \le 64} t_z(a,b)$$

$$g_{max}(a,b) = \max_{1 \le z \le 64} g_z(a,b)$$

5.3 Modified pulse coupled neural network

The PCNN image segmentation can be simplified by (1) making it depend on only few parameters which can be determined from the image statistics and (2) using simple stop mechanism. In this thesis, the PCNN of chapter 4 is modified such that image segmentation depends only on two parameters namely linking coefficient β(m,n) and initial threshold θ_0(m,n) which can be determined from image statistics and for which no stop mechanism is required as the number of iteration is limited to 1 i.e., i_t is equal to1. The equations for modified PCNN are given below:

$$f_{i_t}(m,n) = x(m,n) \tag{5.8}$$

$$l_{i_t}(m,n) = \sum_{i=-1}^{1}\sum_{j=-1}^{1} W(i+2, j+2) \cdot y_{i_t}(m+i, n+j) \tag{5.9}$$

$$u_{i_t}(m,n) = f_{i_t}(m,n) \cdot \left(1 + \beta(m,n) \cdot l_{i_t}(m,n)\right) \tag{5.10}$$

$$y_{i_t}(m,n) = \begin{cases} 1 \text{ if } u_{i_t}(m,n) \geq \theta_{i_t-1}(m,n) \\ 0 \; otherwise \end{cases} \tag{5.11}$$

The linking coefficient and initial threshold are calculated using methods described in section 5.2. The algorithm used for image segmentation using modified PCNN is as follows:

Step 1: Initialization:

Initialize values of arrays f, l, u, θ and s of size M×N to 0 (i.e. for n=0).

Initialize weight matrix [8] $\mathbf{W}=\begin{bmatrix} 0.5 & 1 & 0.5 \\ 1 & 0 & 1 \\ 0.5 & 1 & 0.5 \end{bmatrix}$

Initialize the iteration number i_t =1, row and column variable m and n to 1.

Step 2: Calculate linking coefficient $\beta(m,n)$ and initial threshold $\theta_0(m,n)$ value of the image using equation (5.1) and algorithm described in section 5.2.2.

Step 3: Calculate the feeding input using equations (5.8).

Step 4: Calculate the linking input, internal activation value and output using equation (5.9), (5.10) and (5.11) respectively.

Step 5: n=n+1. If n≤N go to step 3, else go to step 6.

Step 6: n=1,m=m+1.If m≤M go to step 3, else go to step 7.

Step 7: Save array **y** as the segmented image.

5.4 Silicon wafer defect segmentation using modified PCNN

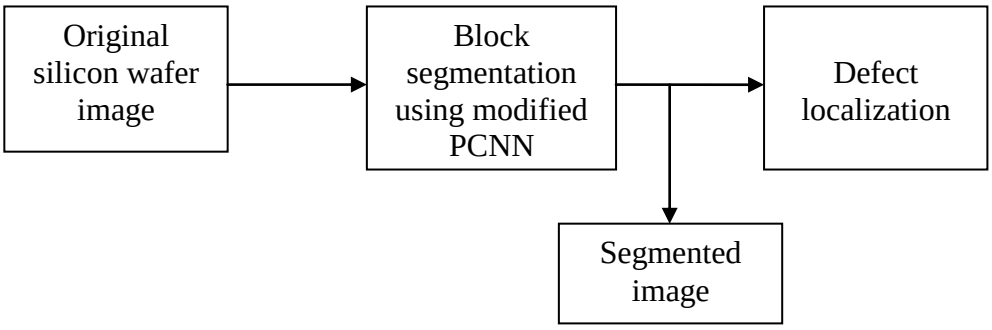

Figure 5.2 Block segmentation of silicon wafer defect using modified PCNN

The three steps involved in silicon wafer defect segmentation using modified PCNN are: (1) Input image (2) Block segmentation using modified PCNN and (3) Defect localization. In first step silicon wafer image is input to the system. In second step input image x(m,n) of size MxN is block segmented using modified PCNN described in section 5.3 with parameters linking coefficient $\beta(a,b)$ and initial threshold $\theta_0(a,b)$ obtained using algorithms described in section 5.2.1 and 5.2.2 respectively. In the final step the defect localization is done using method described in section 2.4.

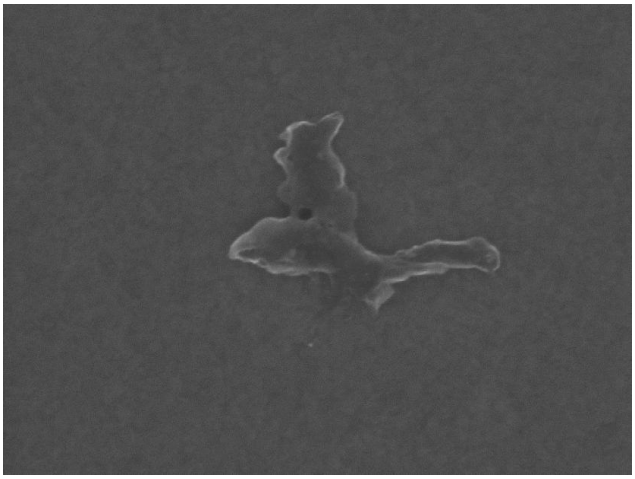

Figure 5.3 Silicon wafer image with plastic defect

The image shown in the figure 5.3.with plastic defect is used as input image for segmentation using modified PCNN. It can be observed there is intensity overlap between defect region and the background and a global threshold cannot be used for segmentation. This image can be segmented effectively using modified PCNN.

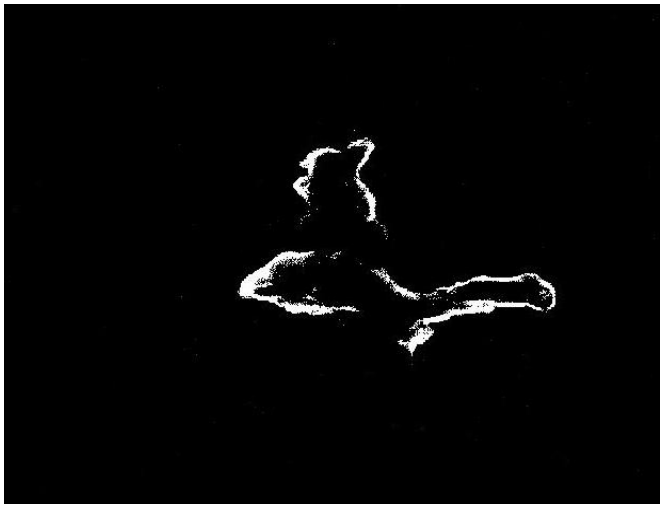

Figure 5.4 Segmented image obtained after removing block effect

The segmented image shown in figure 5.4 contains a plastic defect only in contrast to the image of figure 5.4. It can be observed the threshold adjusted using local deviation of contrast parameter has resulted in proper segmentation of the defect. This segmented image with only defect pixels can be used for defect localization.

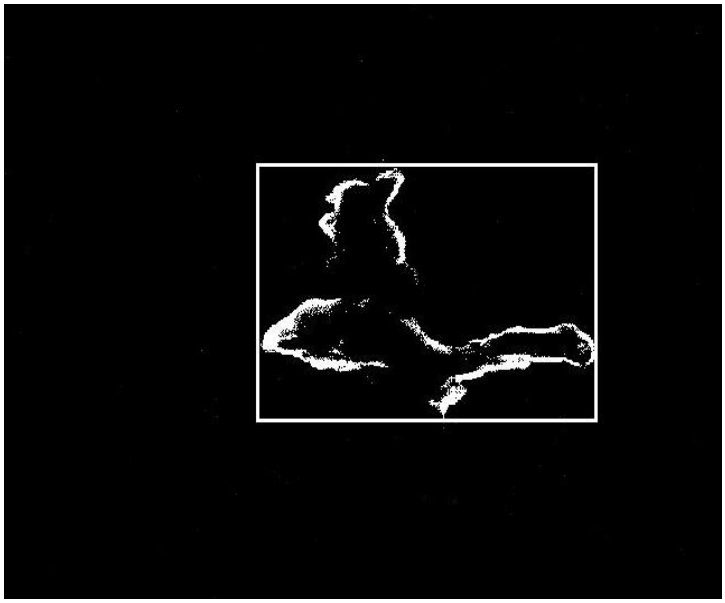

Figure 5.5 Defect localized image

The localized image obtained after applying localization process is shown in figure 5.7. Different features can be extracted from this image which is used for defect recognition. Silicon defect segmentation system based on modified PCNN is used to segment four types of silicon wafer defects. The defects include Copper ball defect, plastic defect, pit defect and protrusion defect. The system is capable of segmenting these defects efficiently. The chapter 6 discusses segmentation results of four silicon wafer defects.

CHAPTER 6

RESULTS

In this chapter, the algorithm developed in this thesis is compared to Otsu's method and to the original PCNN approach. These algorithms were implemented in MATLAB R2008b.

6.1 Copper ball defect dataset

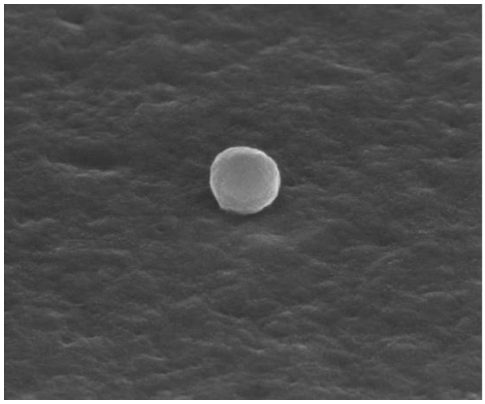

Figure 6.1 Copper ball defect image

An input image with a copper ball defect is shown in figure 6.1. It can be observed that intensities of defect pixels are higher than those of background pixels, which results in a bimodal histogram distribution.

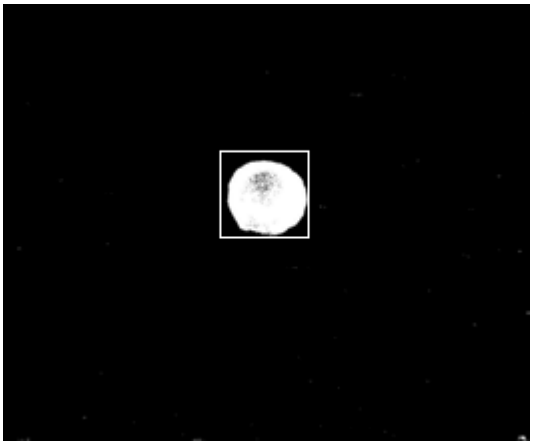

Figure 6.2 Image obtained using Otsu's method

The localized defect obtained using Otsu's method is shown in figure 6.2. It can be observed that the segmentation was effective because of large difference in intensity between defect region and background of the image and for which optimal threshold was obtained.

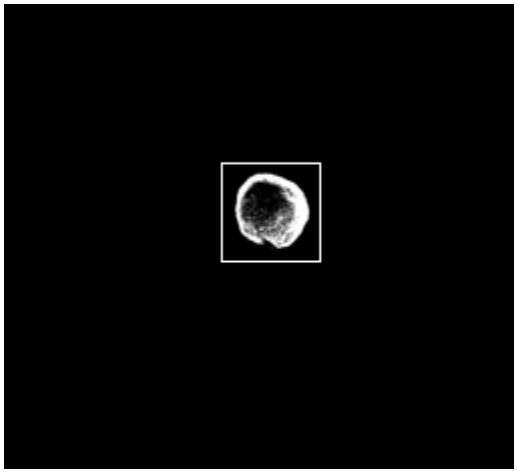

Figure 6.3 Image obtained using PCNN

The localized defect obtained using PCNN is shown in figure 6.3. It can be observed that the defect is not segmented properly which is due to global initial threshold value and linking coefficient.

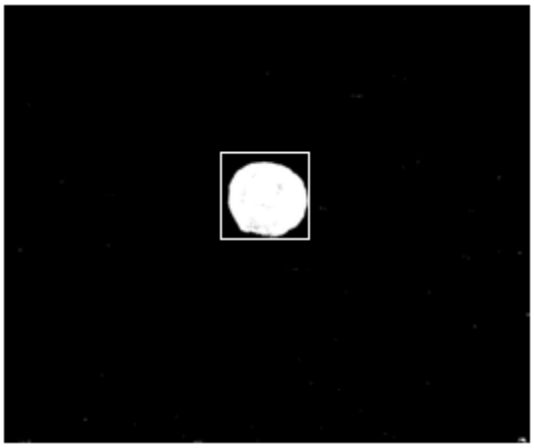

Figure 6.4 Image obtained using modified PCNN

The localized defect in figure 6.4 obtained using modified PCNN has the defect segmented effectively compared to figure 6.3 because different initial thresholds and linking coefficients are used for different regions of the image. It can be observed that the defect is segmented more effectively compared to Otsu's method and the modified PCNN. Comparison of results for the three methods is shown in table 6.1.

Table 6.1 Comparison of results obtained using Otsu's method, PCNN and modified PCNN for copper ball dataset

Method	**Number of correctly segmented images**	**Number of incorrectly segmented images**	**Percentage correctly segmented images**
Otsu's method	24	9	72.72
PCNN	26	7	78.78
PCNN combined method	33	0	100.00

It can be observed from the table 6.1 that the modified PCNN has segmented all defect images in copper ball defect dataset effectively compared to Otsu's method and PCNN

method. Hence, the modified PCNN method is reliable for segmenting the copper ball dataset.

6.2 Plastic defect dataset

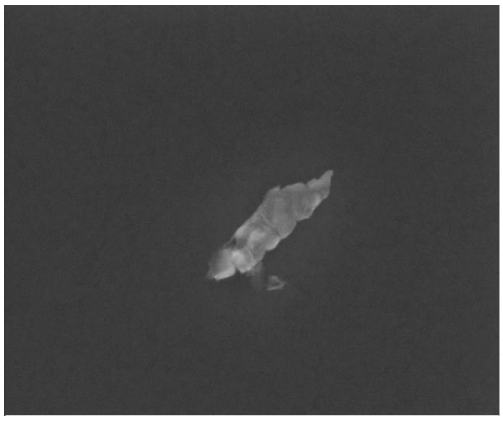

Figure 6.5 Original image

An input image with plastic defect is shown in the figure 6.5. It can be observed that the some regions of the defect have pixel intensity values similar to background pixels.

Figure 6.6 Image obtained using Otsu's method

Due to overlap of intensity range for defect and background of the image in figure 6.5 it is difficult to obtain optimal threshold using Otsu's method and only part of the defect is segmented. So, Otsu's method is not reliable for plastic defect images.

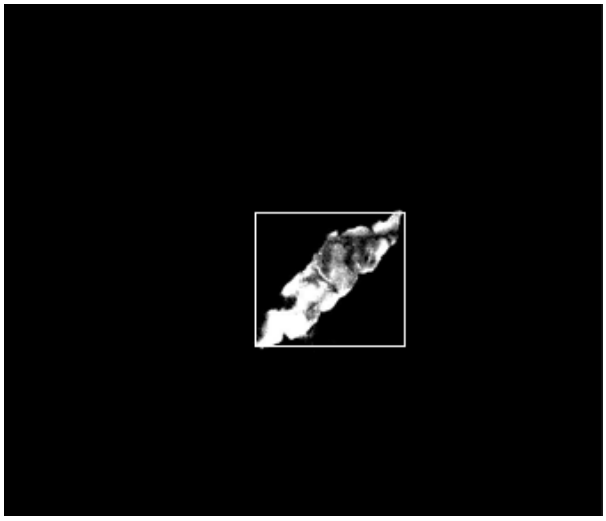

Figure 6.7 Image obtained using PCNN

The PCNN segmented image in figure 6.7 contains defect with few missing defect pixels. It can be observed that the problem of intensity overlap between background and defect regions is overcome in PCNN method because of its linking property.

Figure 6.8 Image obtained using modified PCNN

The modified PCNN segmented image in figure 6.8 contains complete defect. It can be observed that different linking coefficient and initial threshold for different region of the plastic defect image has resulted in good segmentation.

Table 6.2 Comparison of results obtained using Otsu's method, PCNN and modified PCNN for plastic defect dataset

Method	**Number of correctly segmented images**	**Number of incorrectly segmented images**	**Percentage correctly segmented images**
Otsu’s method	3	19	13.64
PCNN	7	15	31.82
PCNN combined method	22	0	100

It can be observed from the table 6.2 that results obtained using algorithm developed for Plastic defect dataset were more efficient than the results obtained using Otsu’s method and PCNN. Unique characteristics of the modified PCNN make the algorithm developed more relevant and reliable for this defect dataset.

6.3 Protrusion defect dataset

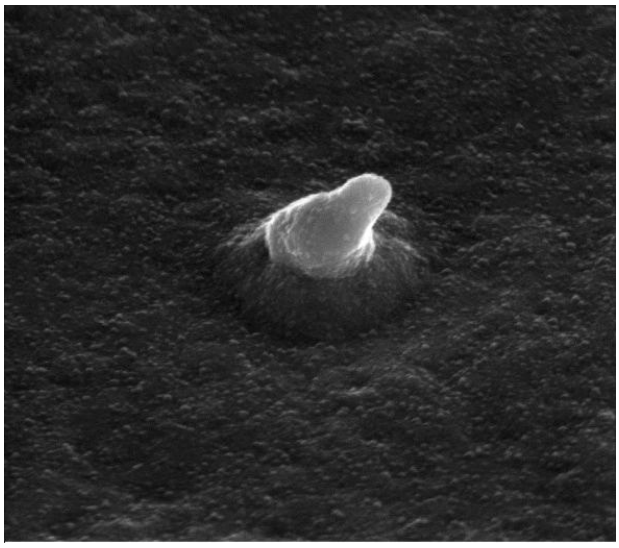

Figure 6.9 Original image

The protrusion defect image in figure 6.9 has defect concentrated in one particular region and with variations in intensity. It can be observed that the large part of the image is occupied by the background pixels.

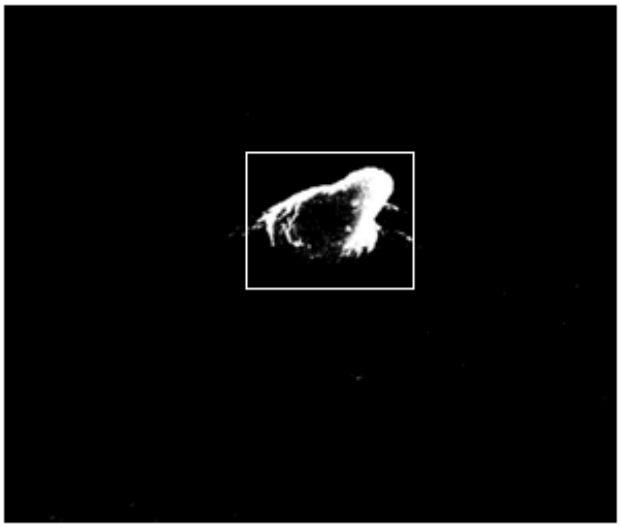

Figure 6.10 Image obtained using Otsu's method

It can be observed from figure 6.10 that due to variations in intensity of defect region an optimal threshold cannot be found which segmented all the pixels of the defect. In figure 6.10 not all defect pixels are segmented using Otsu’s method.

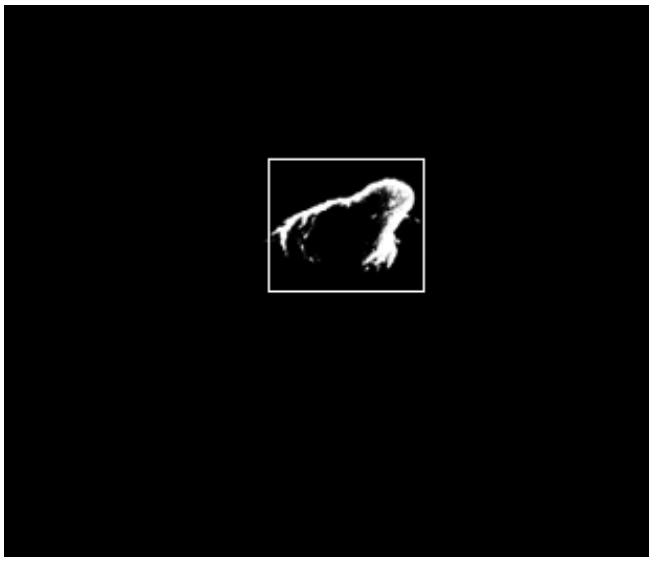

Figure 6.11 Image obtained using PCNN

It can be observed from figure 6.11 that the PCNN segmentation is worse than the Otsu's method. Only few pixels of the defect are segmented as a result of poor linking due to global linking coefficient.

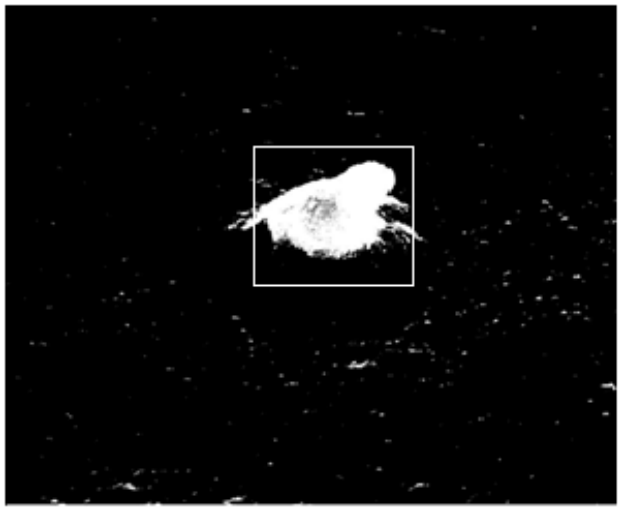

Figure 6.12 Image obtained using modified PCNN

The modified PCNN segmented image in figure 6.12 has the complete defect region. It can be observed that the variations in intensity of defect pixels dealt with different linking coefficient of modified PCNN.

Table 6.3 Comparison of results obtained using Otsu's method, PCNN and modified PCNN for protrusion defect dataset

Method	**Number of correctly segmented images**	**Number of incorrectly segmented images**	**Percentage correctly segmented images**
Otsu's method	4	7	36.36
PCNN	8	3	72.72
PCNN combined method	11	0	100

The results in table 6.3 show that the performance of the modified PCNN for protrusion defect dataset is better than the Otsu's method and PCNN method. Hence, the modified PCNN method is reliable for protrusion defect image segmentation.

6.4 Pit defect dataset

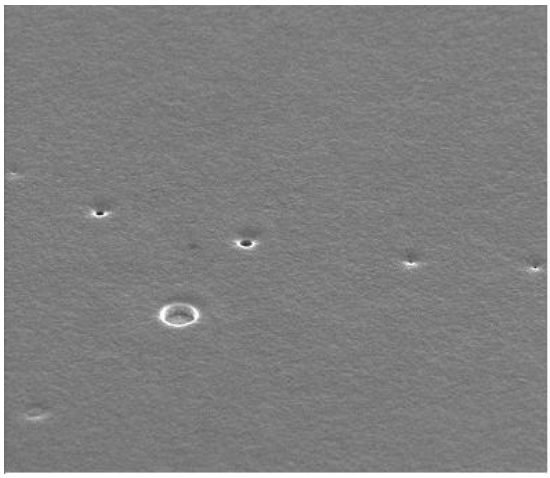

Figure 6.13 Original image

An input image with pit defect is shown in figure 6.13. It can be observed that the area of the defect region is small and some defect pixels with less intensity value compared to background pixels.

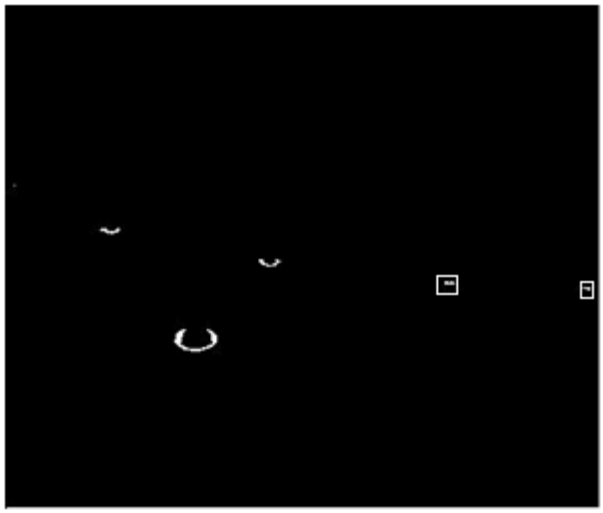

Figure 6.14 Image obtained using preprocessing and Otsu's method

Otsu's segmented image in figure 6.14 contains part of the defects. Due to large intensity variations in the defect regions it is difficult to find an optimal Otsu's threshold for the segmentation. Hence, Otsu's method failed to segment pit defect images effectively.

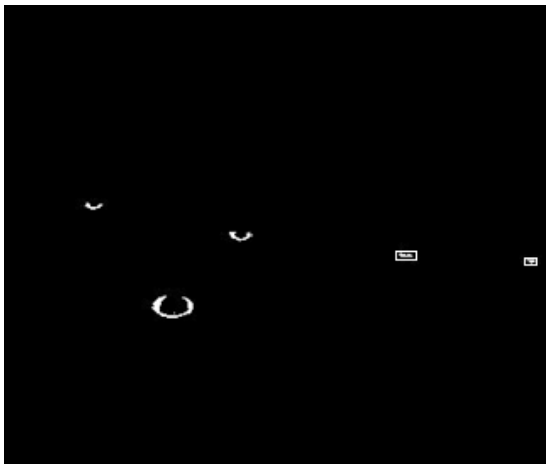

Figure 6.15 Image obtained using PCNN

As shown in figure 6.15 PCNN segmented image is better than Otsu's method. It can be observed that the large intensity variations in defect regions are dealt with linking property of PCNN. But still some defect pixels are segmented as background because a global initial threshold is used.

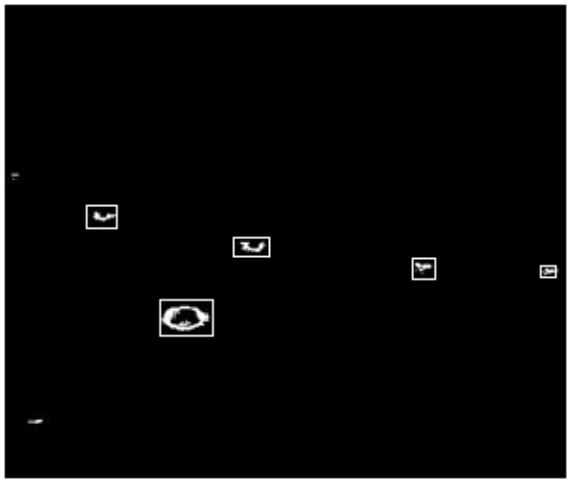

Figure 6.16 Image obtained using modified PCNN

It can be seen in figure 6.16 that all defects are localized because different initial threshold and linking coefficient are used for different regions of the defect image. The modified PCNN segmented image is better than PCNN and Otsu's methods.

Table 6.4 Comparison of results obtained using Otsu's method, PCNN and modified PCNN method for pit defect

Method	**Number of correctly segmented images**	**Number of incorrectly segmented images**	**Percentage correctly segmented images**
Otsu's method	2	3	40.00
PCNN	2	3	40.00
PCNN combined method	4	1	80.00

The results in table 6.4 show that performance of the algorithm developed was better than both Otsu's method and the original PCNN. The percentage of the correctly segmented images was more for the algorithm developed than both Otsu's method and PCNN. Hence, modified PCNN is reliable method for segmenting pit defect dataset.

CHAPTER 7

CONCLUSIONS AND FUTURE WORK

7.1 Conclusion

In this thesis, several prospects of improving image segmentation process using the modified pulse coupled neural network are explored. The performance of modified pulse coupled neural network was found to be better than the traditional image segmentation methods. Modified pulse coupled neural network used was simplified version of traditional PCNN and for which image segmentation depends only on linking coefficient and initial threshold. With only two parameters affecting the segmentation process modified PCNN was found reliable for silicon defect segmentation. The automatic determination of these two network parameters values from image statistics is dealt with efficiently using threshold value obtained from Otsu's method and linking coefficient value obtained for method described in [17]. The large intensity variations involved in silicon defect segmentation are dealt with adaptive segmentation using modified PCNN. The problem of applying appropriate stop mechanism for determining best segmented image is overcome by using single iteration in modified PCNN. It was found that the same algorithm worked well for all four types of silicon defects. Although the algorithm is complex compared to traditional image segmentation techniques the results obtained

were reliable. Hence, reliable algorithm for silicon defect segmentation was developed in this thesis.

7.2 Future work

Given the draw backs of the pulse coupled neural networks – namely non-linear mechanism, dependence of segmentation results on network parameters, it necessary to find better method to determine all the networks parameters from the image statistics so that more accurate segmented results can be obtained. It is suggested to have a method to determine automatically if there is any requirement for block segmentation or not. And, it should be possible to determine number of blocks into which the image must be partitioned for block segmentation method. Future work should focus on automating the block segmentation of the image and determining all the network parameters from the image statistics.

REFERENCES

[1] Karin Sobottka, Ioannis Pitas, “Segmentation and Tracking of Faces in Color”, Proceedings of second International Conference on Automatic Face and Gesture Recognition, Killington, Vermont, Oct. 1996, pp. 236-241.

[2] Pham, D., Xu, C., and Prince, J., 2000. Current Methods in Medical Image Segmentation. Annual Review of Biomedical Engineering 2, 315-337.

[3]Hassanien, A.E.; Ali, J.M.; , "Digital mammogram segmentation algorithm using pulse coupled neural networks," Image and Graphics, 2004. Proceedings. Third International Conference on , vol., no., pp. 92- 95, 18-20 Dec. 2004

[4] Gaceb, D.; Eglin, V.; LeBourgeois, F.; Emptoz, H.; , "Physical Layout Segmentation of Mail Application Dedicated to Automatic Postal Sorting System," Document Analysis Systems, 2008. DAS '08. The Eighth IAPR International Workshop on , vol., no., pp.408-414, 16-19 Sept. 2008

[5]Khan, M.A.; Khan, M.K.;"Improved fingerprint identification using directional filter banks," Multi Topic Conference, 2003. INMIC 2003. 7th International , vol., no., pp.49-54, 9-9 Dec. 2003

[6] Thammakaroon, P.; Tangamchit, P.; "Predictive brake warning at night using taillight characteristic," Industrial Electronics, 2009. ISIE 2009. IEEE International Symposium on , vol., no., pp.217-221, 5-8 July 2009

[7] Ting-lei Huang; Xue Bai;"An Improved Algorithm for Medical Image Segmentation," Genetic and Evolutionary Computing, 2008. WGEC '08. Second International Conference on , vol., no., pp.289-292, 25-26 Sept. 2008

[8] Ma Yi-de; Liu Qing; Qian Zhi-bai; , "Automated image segmentation using improved PCNN model based on cross-entropy," Intelligent Multimedia, Video and Speech Processing, 2004. Proceedings of 2004 International Symposium on , vol., no., pp. 743-746, 20-22 Oct. 2004

[9] Nikhil R Pal, Sankar K Pal, A review on image segmentation techniques, Pattern Recognition, Volume 26, Issue 9, September 1993, Pages 1277-1294, ISSN 0031-3203,

[10] Kuntimad, G.; Ranganath, H.S.; , "Perfect image segmentation using pulse coupled neural networks," Neural Networks, IEEE Transactions on , vol.10, no.3, pp.591-598, May 1999

[11] Xiaodong Gu; Liming Zhang; Daoheng Yu; , "General design approach to unit-linking PCNN for image processing," Neural Networks, 2005. IJCNN '05. Proceedings. 2005 IEEE International Joint Conference on , vol.3, no., pp. 1836- 1841 vol. 3, 31 July-4 Aug. 2005

[12] Zhong Zhang, “Blum R.S.A categorization of multiscale-decompositionbased image fusion schemes with a performance study for a digitalcamera application,” Proceedings of the IEEE, vol.87, no.8, pp.1315-1326, Aug.1999.

[13] Yamada, H.; Ogawa, Y.; Ishimura, K.; Wada, M.; , "Face detection using pulse-coupled neural network," SICE 2003 Annual Conference , vol.3, no., pp. 2784- 2788 Vol.3, 4-6 Aug. 2003

[14] Sadjadi, F.;"Polarimetric IR automatic target detection and recognition," Acoustics, Speech, and Signal Processing, 1996. ICASSP-96. Conference Proceedings., 1996 IEEE International Conference on , vol.4, no., pp.2140-2143 vol. 4, 7-10 May 1996

[15] F. Z. Kettaf, D. Bi, and J. P. Asselin de Beauville , "A comparison study of image segmentation by clustering technique s", IEEE Trans, vol. 2,1996, pp. 1280-1283.

[16] Awad, M.M.; Nasri, A.; , "Satellite image segmentation using Self- Organizing Maps and Fuzzy C-Means," Signal Processing and Information Technology (ISSPIT), 2009 IEEE International Symposium on , vol., no., pp.398-402, 14-17 Dec. 2009

[17] Xiaojun Jia; , "A novel segmentation method using improved PCNN for fabric defect image," Signal Processing Systems (ICSPS), 2010 2nd International Conference on , vol.1, no., pp.V1-388-V1-392, 5-7 July 2010

[18] Ng, H.P.; Ong, S.H.; Foong, K.W.C.; Goh, P.S.; Nowinski, W.L.; , "Medical Image Segmentation Using K-Means Clustering and Improved Watershed Algorithm," Image Analysis and Interpretation, 2006 IEEE Southwest Symposium on , vol., no., pp.61-65, 0-0 0

[19] R. C. Gonzales, R. E. Woods, and S. L. Eddins, Digital Image Processing using MATLAB, Pearson Education, 2008.

[20] Milan Sonka, Vaclav Hlavac, Roger Boyle, Image processing, Analysis and Machine vision, Thomson Brooks/Cole, second edition.

[21] Mahinda Pathegama & Ö Göl (2004): "Edge-end pixel extraction for edge-based image segmentation", Transactions on Engineering, Computing and Technology, vol. 2, pp 213-216, ISSN 1305-5313

[22] R. Eckhorn, H.J. Reitboeck, M. Arndt, P.W. Dicke, A neural network for feature linking via synchronous activity: results from cat visual cortex and from simulations, in: Models of Brain Function,Cambridge University Press,Cambridge, UK, 1989, pp. 255–272.

[23] Lindblad, Th. and Kinser, J. M. Image Processing using Pulse- Coupled Neural Networks, *Perspectives In Neural Computing*. Springer-Verlag Limited. ISBN 3-540-76264-7.

[24] H.S. Ranganath, G. Kuntimad, J.L. Johnson, Pulse coupled neural networks for image processing, in: Proc. of the Southeast Conference on 'Visualize the future', 1995, pp. 37–43.

[25] J. L. Johnson, "Pulse-coupled Neural Networks,,'Adaptive Computing: Mathematics,Electronics and Optics, Vol CR55, Proc of a conference held 4-5 April 1994, Orlando FL.

[26] Y. Ma, F. Shi, L. Li, A new kind of impulse noise filter based on PCNN, in: Proc.of International Conference on Neural Networks and Signal Processing, vol. 1,2003, pp. 152–155.

[27] M. Shi, J. Zhang, Y. Li, D. Wu, A new method of low contrast image enhancement, Computer Engineering and Applications (1) (2005) 235–238.

[28] G. Li, H. Li, T. Wu, M. Dong, Applications of PCNN and Otsu theories for image enhancement, Journal of Optoelectronics Laser 16 (3) (2005) 358–362.

[29] G. Li, H. Li, T. Wu, Enhancement of image based on Otsu and modified PCNN, Journal of System Simulation 17 (6) (2005) 1370–1372.

[30] G. Li, H. Li, T. Wu, The image enhancement based on modified pulse coupled neural network and genetic algorithm, Journal of Test and Measurement Technology 19 (3) (2005) 304–309.

[31] J. Lu, L. Fang, Y. Ye, X. Yang, Z. Cheng, Infrared image enhancement based on pulse-coupled neural network, Opto-Electronic Engineering 34 (2) (2007) 50–54.

[32] D. Feng, Z. Yang, Z. Wang, Adaptive enhancement algorithm of color image based on improved PCNN, in: Proc. of the 8th International Conference on Electronic Measurement and Instruments, vol. 2, 2007, pp. 844–848.

[33] R.P. Broussard, S.K. Rogers, M.E. Oxley, G.L. Tarr, Physiologically motivated image fusion for object detection using a pulse coupled neural network, IEEE Transactions on Neural Networks 10 (3) (1999) 554–563.

[34] Q. Miao, B. Wang, A novel algorithm of multi-focus image fusion using adaptive PCNN, Journal of Electronics and Information Technology 28 (3) (2006) 466–470.

[35] W. Huang, Z. Jing, Multi-focus image fusion using pulse coupled neural network, Pattern Recognition Letters (2007) 1–10.

[36] Hui-Fuang Ng; , "Automatic thresholding for defect detection," *Image and Graphics, 2004. Proceedings. Third International Conference on* , vol., no., pp. 532- 535, 18-20 Dec. 2004

[37] Ge, J.; Wang, Y.; Zhou, B.; Zhang, H. Intelligent Foreign Particle Inspection Machine for Injection Liquid Examination Based on Modified Pulse-Coupled Neural Networks**.** Sensors 2009**,** 9**,** 3386-3404.

[38] Forgac, R.; Mokris, I.; , "Algorithm for Pulse Coupled Neural Network parameters estimation," *Computational Cybernetics, 2009. ICCC 2009. IEEE International Conference on* , vol., no., pp.147-151, 26-29 Jan. 2009

[39] Peng, Z., Jiang, B., Wang, H., Aerial target detection using improved ULPCNN combining with contour tracking, 2nd International Symposium on Photoelectronic Detection and Imaging: Image processing. Proc. SPIE, vol.6623, Bejing, p.6620D

[40] Reyes, A. and Constantino, C.: Image Segmentation with Kohonen Neural Network Self Organizing Maps. In *International Conference on Telecommunications ICT 2000*, Acapulco, Mexico, 2000.

[41] Gu Xiaodong; Zhang Liming; , "Morphology open operation in unit-linking pulse coupled neural network for image processing," *Signal Processing, 2004. Proceedings. ICSP '04. 2004 7th International Conference on* , vol.2, no., pp. 1597- 1600 vol.2, 31 Aug.-4 Sept. 2004

[42] Zhaobin Wang, Yide Ma, Feiyan Cheng, Lizhen Yang, Review of pulse-coupled neural networks, Image and Vision Computing, Volume 28, Issue 1, January 2010, Pages 5-13, ISSN 0262-8856

[43] Grimson, W.E.L.; Ettinger, G.J.; White, S.J.; Lozano-Perez, T.; Wells, W.M., III; Kikinis, R.; , "An automatic registration method for frameless stereotaxy, image guided surgery, and enhanced reality visualization," *Medical Imaging, IEEE Transactions on* , vol.15, no.2, pp.129-140, Apr 1996

[44] Xiaolan Zeng; Staib, L.H.; Schultz, R.T.; Duncan, J.S.; , "Segmentation and measurement of the cortex from 3-D MR images using coupled-surfaces

propagation," *Medical Imaging, IEEE Transactions on* , vol.18, no.10, pp.927-937, Oct. 1999

[45] D. L. Pham, C. Y. Xu, and J. L. Prince, “Current methods in medical image segmentation,” *Annu. Rev. Biomed. Eng.*, vol. 2, pp. 315–337, Aug.2000.

[46] H. Bai, Y. Kang, and C. C. Liu, “Dimensional and elemental analysis of particulate contaminations on silicon wafers,” *Aerosol Air Qual. Res.*,vol. 2, no. 1, pp. 53–60, 2002.

[47] Kuang-Peng Lin; Kai-Ming Ching; Kwo-Shu Huang; Shun-Liang Hsu; , "A study of implant damage induced thin oxide film expansion during photoresist dry etching," *Reliability Physics Symposium, 2000. Proceedings. 38th Annual 2000 IEEE International* , vol., no., pp.404-406, 2000]

[48] C. L. Claeys, High silicon purity V, The Electrochemical Society, 1998,pp.213-247.

[49] P. Rai-Choudhury, Proceedings of the Electrochemical Society Symposium on Diagnostic Techniques for Semiconductor Materials and Devices, The Electrochemical Society, 1997.pp 192-240.

[50] MA Yide, DAI Rolan, et al. Image segmentation of embryonic plant cell using pulse-coupled neural networks. Chinese Science Bulletin, 2002, 47(2): 167-172.

BIOGRAPHICAL INFORMATION

Chaitanya Telidevara was born in India in 1986. He did his Bachelor of Technology in Biomedical Engineering from Jawaharlal Nehru Technological University, Hyderabad in May 2008. He obtained his Master of Science degree from the University of Texas at Arlington in May 2011. He is also a member and active officer of the UTA chapter of Tau Beta Pi engineering honor society. His current research interests include image processing and pattern recognition.